ENERGY CONVERSION AND MANAGEMENT
https://doi.org/10.1016/j.enconman.2020.112549/

CONTROL STRATEGY OPTIMIZATION OF A STIRLING BASED RESIDENTIAL HYBRID SYSTEM THROUGH MULTI-OBJECTIVE OPTIMIZATION

Aritz Bengoetxea[1], Marta Fernandez[1,2], Estibaliz Perez-Iribarren[1], Iker Gonzalez-Pino[1], Jesus Las-Heras-Casas[3], Aitor Erkoreka[1]

[1]ENEDI Research Group, Department of Thermal Engineering, University of the Basque Country (UPV/EHU), Alda. Urquijo s/n, 48013 Bilbao, Spain. Corresponding author e-mail: bengoetxea93@gmail.com

[2]Department of Mechanical Engineering, Heat Engines and Fluid Mechanics, School of Industrial Engineering, University of Vigo, 36310 Vigo, Spain.

[3]TENECO Research Group, Department of Mechanical Engineering, University of La Rioja, Calle San Jose de Calasanz, 31, 26004, Logroño, La Rioja, Spain

Abstract:

Hybrid systems for space heating and Domestic Hot Water (DHW) production are an attractive option for buildings to decrease their CO_2 emissions. In this research, the operation variables of an installation, composed of a Stirling engine, a condensing boiler and a thermal storage tank, were optimized to supply heating and DHW demands of a virtual detached house. For this purpose, in an experimental installation operated with common control set points, the hybrid system was tested during the week of highest demand. Then the installation was modelled in TRNSYS, calibrated and validated against the experimental data and, finally, different multi-objective optimizations were carried out on the model to optimize the operation set points.

The results obtained show that solely by optimizing the control variables of the calibrated model of the actual installation gives a reduction of 7% in cost and an improvement of 3.9% in exergy efficiency. Thus, it can be concluded that simply optimizing control variables in this type of hybrid systems can lead to low cost reductions. By reducing the thermal losses of the calibrated model from the experimental 17% of energy consumed to 5% and then optimizing it, a reduction of 17% in cost and an improvement of 23% in exergy efficiency were obtained. Different model insulation levels were tested, and two interesting conclusions were found from this analysis: until the level of transmission losses is below 5% of the energy consumed, the optimized operation conditions lead to a negligible use of the thermal storage, after which it increases drastically. On the other hand, it can be concluded that the cost optimization that optimizes the adiabatic model of the analysed hybrid system is insensitive to the selected control variables.

HIGHLIGHTS:

- Reduction of 7% in the cost of the Stirling based hybrid system.
- Increase of 3.9% in the exergy efficiency of the Stirling based hybrid system.
- Optimized cost of the ideal adiabatic model of the hybrid system is insensitive to the control variables.
- The installation's optimized operating set points are very sensitive to the level of thermal losses of the storage system.
- The use of the optimized storage system is only interesting for cases with low transmission losses.

KEYWORDS:

Micro-Combined Heat and Power, hybrid installation, thermal insulation, thermal energy storage, multi-objective optimization.

NOMENCLATURE

c_E	Cost of the electricity [€/kWh]	CHP	Combined Heating and Power
c_F	Cost of the natural gas consumption [€/kWh$_{LHV}$]	$CV\ (RMSE)$	Coefficient of Variation of the Root Mean Square Error
c	Specific heat [kJ/kg K]	DHW	Domestic Hot Water
E_{CHP}	Electricity generated by the micro-CHP [kWh]	GA	Genetic Algorithm
Ex_{DHW}	Exergy dissipated in the DHW plate exchanger in each time-step [kWh]	GHG	Greenhouse Gas Emissions
$Ex_{heating}$	Exergy dissipated in the fan coil due to heating in each time-step [kWh]	HC	Hydraulic Compensator
F_{BOI}	Fuel consumption of the condensing boiler [kWh$_{LHV}$]	HT-PEM	High temperature polymer electrolyte
F_{CHP}	Fuel consumption of the micro-CHP [kWh$_{LHV}$]	LCCE	Laboratory for the Quality Control of Buildings of the Basque Government
$\dot{m}$	Mass flow rate [kg/s]	LHV	Lower Heating Value
r_{ex-e}	Fuel exergy-energy ratio	Micro-CHP	Micro-Combined Heating an Power
T_{AVG}	Average temperature [ºC]	MINLP	Mixed Integer Non Linear Programming
T_{BOI}	Outlet temperature of the boiler [ºC]	NG	Natural Gas
T_{CHP}	Outlet temperature of the micro-CHP [ºC]	NSGA-II	Non-dominated Sorting Genetic Algorithm-II
T_{ret_CHP}	Return temperature of the micro-CHP [ºC]	ORC	Organic Rankine Cycle
T_{TANK}	Temperature of the thermal energy storage [ºC]	PEMFC	Proton Exchange Membrane Fuel Cell
ΔT_{charge}^{ON}	Difference of temperatures to switch ON the charge [ºC]	SE	Stirling Engine
ΔT_{charge}^{OFF}	Difference of temperatures to switch OFF the charge [ºC]	TES	Thermal Energy Storage
$\Delta T_{discharge}^{ON}$	Difference of temperatures to switch ON the discharge [ºC]	V2V	Two-way valve
$\Delta T_{discharge}^{OFF}$	Difference of temperatures to switch OFF the discharge [ºC]	V3V	Three-way valve

Greek symbols

ψ	Exergy performance of the plant

1 Introduction

Nowadays, one of the foremost concerns worldwide is increasing energy consumption. Residential and commercial buildings account for 40% of the energy consumed and 36% of greenhouse gas emissions (GHG) in Europe [1]; while in Spain, this sector is in third place for final energy consumption with 17% [2]. Consequently, in the past few decades, much research has sought the reduction of energy consumption and the development of technologies that generate power more efficiently, in a way that is less harmful to the environment [3]. In the residential-commercial sector, these solutions focus on improving the building envelope or the efficiency of thermal systems.

With this aim, micro-CHP (Combined Heating and Power) technologies have great potential for use in residential buildings, as can be seen in the reviews presented in [4, 5]. They provide thermal energy and electricity jointly, which are the main energy demands of these buildings. Besides, their use brings multiple economic and environmental advantages, such as greater efficiency in the generation system, leading to reductions in the annual energy cost and GHG emissions, along with a decrease in transport losses or an improvement in the quality of energy supply. In [6], the non-renewable primary energy consumption of a residential micro-CHP engine is compared with two different scenarios where electricity and heat are obtained from different sources. The first scenario considers a boiler used to supply the heat demand, while the electricity is obtained directly from the grid (considering the European production mix). The second scenario considers the same boiler for heat, while the electricity is also taken from the grid, but is assumed to be produced solely by combined cycle power plants. The results show that the use of micro-CHP against the first scenario gives global non-renewable primary energy consumption

reductions of up to 34%, and 14% compared with the second. The latter values assume that electricity grid losses represent 11.7%.

Some of the different existing CHP technologies for applications on a domestic scale are fuel cells, micro turbines, internal combustion engines, Organic Rankine Cycle (ORC) systems [7] and external combustion engines, such as the Stirling Engine (SE) [8]. In this work, a technology based on SE is used. These technologies are used in many applications, such as solar generation, cryogenic or micro-CHP [9]. This technology is classified as an external combustion engine and its efficiency, in theory, is limited by the Carnot cycle. The SE separates the combustion process from the working fluid and allows the provision of continuous heat input to the working gas, with a more controllable combustion, resulting in low pollutant emissions and high combustion efficiency, while also being clean and quiet. Instead of combustion products, the heat source can also come from other sources, such as in solar dish Stirling CHP systems [10]. Lately, this technology has been widely studied for its application in residential buildings [11]. SE for residential buildings is seen as a replacement for traditional gas boiler systems. This technology is well suited to fulfil these requirements when supplying heating, DHW and electric power in the household sector. Over the last few years, the main effort has been focused on developing low-powered residential devices suitable for most thermal and electric demands in single family houses.

The installation of cogeneration systems usually requires the support of conventional equipment, such as an auxiliary boiler and a thermal storage system to cover substantial demand peaks [12]. The storage tank considerably reduces the dissipation of useful heat, raising the number of operating hours of the micro-CHP unit. This kind of energy systems are known as hybrid systems.

The optimization of the operation and sizing of the CHP systems acquires a significant relevance in residential or tertiary buildings, mainly due to the variability of the thermal and electrical demands, as well as the market prices. The most appropriate configuration would be the one with the minimum cost and environmental impact; however, on many occasions, these objectives are in conflict [12]. Through the application of a multi-objective approach, it is possible to determine the complete spectrum of solutions that satisfy very diverse objectives, such as economic or thermodynamic ones, or energy and environmental impacts.

Over the last few decades, several methods have been proposed to address optimization problems. On the one hand, mathematical programming methods: Mixed Integer Linear Programming: (MILP) or Mixed Integer Non Linear Programming: (MINLP) [13]. On the other hand, there are heuristic methods: Genetic Algorithms (GA) [14], simulated annealing [15], particle swarm, taboo-search, fuzzy logic [16], dynamic programming [17] or Lagrangian relaxation [18].

Different evolutionary algorithms, which are widely used in many fields, have been developed to solve multi-objective optimization problems, including energy technologies. The work presented in [19] optimizes a cooling tower assisted vapour compression refrigeration system by means of a GA under thermodynamic and economic criteria. Accordingly, [20] optimizes both the total irreversibility rate and the total product cost of a vapour compression–absorption cascaded refrigeration system using a GA technique. Wang et al. [21] present an algorithm based on evolutionary algorithms for sizing a hybrid renewable energy system. The non-dominated sorting Genetic Algorithm-II (NSGA-II), proposed by Deb et al. [22], is a commonly used algorithm for building performance optimization as well as for building facilities, as can be seen in the studies carried out in the following works [23, 24]. It uses an efficient non-dominated sorting

procedure with an elitist approach, which provides well distributed Pareto solutions [25], so NSGA-II is the optimization algorithm selected in this study to perform the multi-objective optimization approach.

Several works of research can be found in the literature where the design or operative parameters of a Stirling engine are optimized. In [26], an enhanced model of an SE is used to optimize its volume ratio through GA to maximize the thermal efficiency. Xiao [27] studied the performance of the regenerator of an SE, optimizing the regenerator lengths and the heater and cooler tubes to achieve the maximum power output and thermal efficiency. Hachem et al. [9] presents an overview of several Stirling studies, including different technologies, applications and optimization methods applied to an SE.

Furthermore, numerous studies optimize devices within micro-CHP installations or whole micro-CHP installations in domestic buildings. A thermal and economic optimization is presented in Ferreira et al. [10], where a solar dish Stirling cogeneration system applied to a residential building is modelled and optimized at the design stage, by means of the NSGA-II method. Optimizations at the level of whole hybrid installations based on SE can also be found, for example in [28], where a model of a hybrid residential CHP installation composed of a SE, a gas boiler and a TES system is analysed based on not previously calibrated models of the devices. Other works, such as the one presented in [29], also optimize at the level of a whole hybrid installation based on a calibrated model of the SE combined with uncalibrated models of a gas boiler and a TES system.

However, no significant works of research use whole hybrid residential building calibrated and validated installation models to perform an operational optimization of a real in-use micro-CHP system. This work aims to present a methodology to permit the calibration and validation of whole SE based hybrid systems with condensing boiler and

TES system for a further multi-objective optimization of the operating strategies. The methodology is applied to a specific case study of a hybrid experimental plant that fulfils domestic energy needs, consisting of a Stirling-based micro-CHP device together with a conventional boiler and an inertial tank, optimizing its operation variables.

In this research, the SE based micro-CHP system experimental tests were carried out and the plant simulation model was constructed and calibrated using TRNSYS software [30]. The calibrated simulation model was used to apply a multi-objective optimization method with NSGA-II, determining the best control parameters of the aforementioned installation, which enable it to work in the most efficient way possible, according to the different assessed objectives.

The main contributions of this work can be summed up in the following two: On the one hand, it presents a methodology to maximize the exergy efficiency, while minimizing the operational costs of an in-use hybrid system consisting of a Stirling based micro-CHP unit with a condensing boiler and an inertial tank.

On the other hand, it has been found that on uncalibrated whole hybrid residential CHP installation optimizations, the TES system losses are usually considered in two ways. Some research works, such as [28], consider the TES system to be adiabatic, while in other research works, such as [29], the TES system losses are considered within the thermal envelope of the building. Thus, for the optimization technique, losses within the thermal envelope are not losses, but are heat supplied as heating to the building (during the heating season), and that is equivalent to having an adiabatic TES system from the optimization viewpoint. In Spain, it is usual for CHP devices to consider engines installed outside the thermal envelope of the buildings, in very well ventilated spaces. The TES tanks are usually in the same space as the CHP engines, thus considering the thermal

losses of the TES system to be within the building's thermal envelope as useful heat could lead to erroneous optimizations. This is why, in this research, based on the calibrated model of the whole hybrid installation, which considers the real heat losses occurring in the TES tank and the TES system circuit, the influence of the level of the installation's thermal losses on the optimal control variables have been analysed. These results have been found to be of interest for the research community and are presented at the end of the work as a separate section.

2 Methodology

This section starts by presenting the case study where the operational strategy optimization methodology is applied, describing the experimental set up of the hybrid system that has been tested, the test sizing, the control strategy of the experiments and the experimental procedures. Then the installation modelling is presented followed by the installation model calibration and validation procedures. To end this methodology section, the optimization procedure that has been followed is described.

2.1 Case study

The work presented in this article is developed in the experimental plant and built in the Laboratory for Quality Control in Buildings (LCCE) of the Basque Government, located in Vitoria-Gasteiz, Spain. This installation was assembled with the objective of testing the energy performance of individual devices to produce heat, cold and/or electricity (among others: boilers, micro-CHP engines, heat pumps, solar thermal collectors, TES systems and electrical batteries) for the building sector. Furthermore, the installation provides the capacity to hybridize these devices to supply the required heat, cold or electricity demands of a specific building under a specified operation strategy.

During the tests, the specified building heating, cooling or DHW demand is consumed by controlled fan-coils and DHW production. Thus, the energy performance of the hybridized systems can also be evaluated. The installation allows data to be gathered on the operation of tested devices, subject to different operating strategies, and thus the different studied technologies can be evaluated.

2.1.1 Description of the tested hybrid system

The LCCE experimental installation consists of different pieces of equipment grouped into seven modules. Certain devices of the following five modules have been used for this research: High Temperature Generation Module, Distribution Module, Thermal Energy Storage Module, Consumption Module and Acquisition and Control System Module. For clarity, only the hydraulic diagram of the tested hybrid installation is shown in Figure 1.

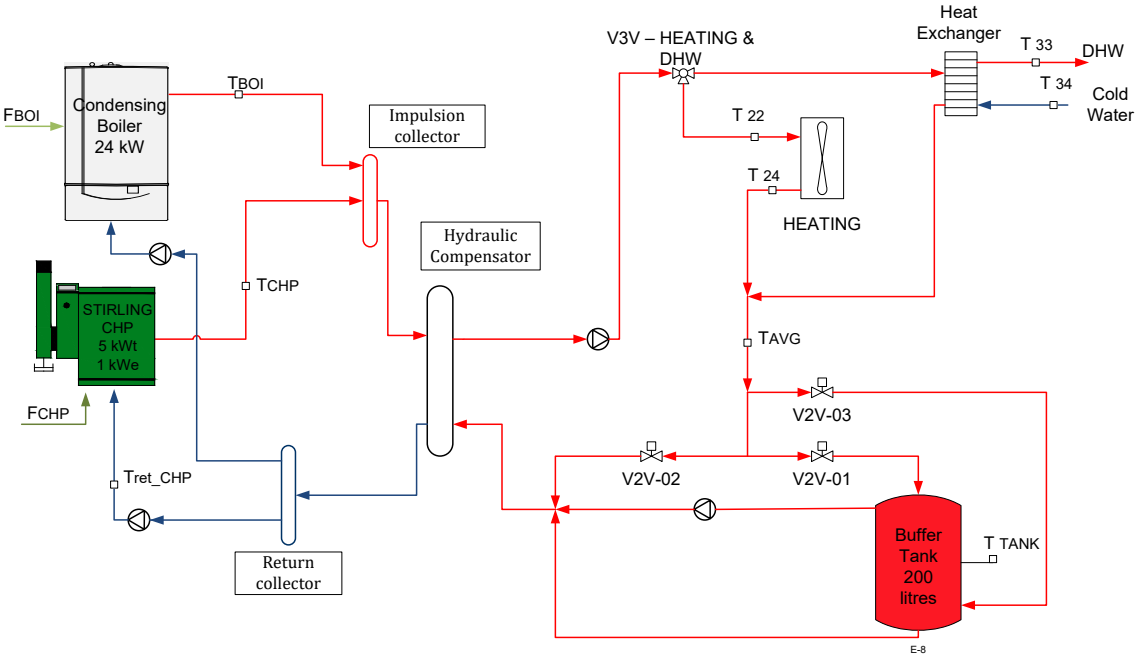

Figure 1. Schematic diagram of the tested hybrid system.

For this research, the High Temperature Generation Module includes two pieces of equipment that work together: a conventional condensing wall boiler, which can work

both at high and low temperatures (see Figure 1 and Figure 2(a)) and a Stirling engine based micro-CHP (Figure 2(b)). The micro-CHP installed is an eVita unit from Remeha, consisting of a mono-cylindrical single piston Stirling engine (1 kWe and 5 kWt) with helium as the working fluid. When there is thermal demand, the Stirling engine is always the first to start up, supplying thermal and electrical power.

The Consumption Module can represent different thermal consumptions required in a residential building. It includes the equipment associated with the Domestic Hot Water (DHW) and heating consumption. To simulate the demand of DHW, a plate exchanger is available in the general DHW circuit, which heats the water through the hot water produced by the Generation Module (see Figure 1). To simulate the heating demand, a heat dissipation unit is used, as shown in Figure 2(d); to be precise, it is a Sedical-Rhoss fan coil unit, model Yardi HP with 5R 250 battery and 2-pipe system, which has a maximum rated thermal power of 24.9 kW with incoming water to 50 °C and up to 42.8 kW when the circulating water temperature is 70 °C.

The Thermal Energy Storage (TES) Module, shown in Figure 2(c), consists of a Vaillant VPS R 200/1 B inertial storage tank with a capacity of 202 litres. To carry out this research, the TES is connected downstream of the consumption module (see Figure 1), so it can be used to accumulate heat when demand is low. The discharge is activated when the tank temperature is higher than a certain programmed value. Table 1 summarizes the main characteristics of the tested devices that belong to each module.

Table 1. Characteristics of the devices of the tested hybrid system

Equipment	Manufacturer	Model	Power	Other
High Temperature Generation Module				
Condensing boiler	BaxiRoca	BIOS 24/28F	24 kW	97 % LHV efficiency (60/80ºC)
Micro-CHP	Remeha	eVita	1 kWe, 5 kWt	Includes a 20 kW auxiliary boiler (disabled for this research)
Distribution Module				
Transfer pump	Grundfos	UPS 40-180 F	--	--
Thermal Energy Storage Module				
TES	Vaillant	VPS R 200/1 B	--	202 litres
Consumption Module				
Plate exchanger	Sedical	UFPB-40/40 H-B-PN25	70 kW	--
Fan coil	Sedical-Rhoss	Yardi HP 5R 250	24.9 kW–50 °C 42.8 kW–70 °C	--

(a)

(b)

(c)

(d)

Figure 2. Images of the experimental equipment: a) condensing boiler, b) micro-CHP, c) TES and d) fan coil.

In total, the Acquisition and Control System of the whole installation includes more than 120 signals to control and monitor the desired variables, so as to obtain accurate information and ensure the proper operation of the installation. Thus, 55 high precision Pt 100 1/10 temperature sensors (47 in pipes and 8 in storage tanks), 11 Siemens SITRANS F M (MAG 3100 and 5100 W sensors and MAG 6000 transmitters) and 2 Magflux 7100 electromagnetic flow-meters with an uncertainty below 0.1% have been installed, as well as electricity meters with a precision of ±1% for the active power, to account for the electrical energy produced by cogeneration and the consumption of the heat pumps. Additionally, the volumetric natural gas flow is determined through a high precision flow meter, whose maximum error is ±0.5%. Thanks to some of these sensors, all the flow rates, all the fuel consumption and electricity production of the SE and the required temperatures for this research have been measured.

The test-bench control is driven by a Siemens IM 151-8 PN/DP CPU programmable logic controller (PLC) and an expansion module, as well as the corresponding signals cards, connected via Ethernet to a personal computer with the interface that the plant is operated through and where the data are acquired. The data from the tests is collected with a frequency of every10 seconds.

2.1.2 Test sizing

This case study was defined to supply the thermal demand of a single-family detached dwelling. The dwelling used is a recently built two-floor single-family house sited in a rural area close to Vitoria-Gasteiz (Northern Spain). It has a thermally conditioned net area of 211.74 m^2 and is located in the D1 climatic zone [31], which is characterized by cold winters and warm summers.

For the purpose of this work, the curves of annual demand for DHW and space heating have been defined for this dwelling in Vitoria-Gasteiz according to the existing bibliography, normative requirements and/or guides and recommendations [32]. The heating demand of the detached dwelling is obtained by an hourly simulation carried out in TRNSYS, where the geometrical and construction information, as well as the internal gains, were introduced according to [33]. Figure 3 represents the monthly heating demand, which rises to 22,154 kWh per year. It can be seen that no heating requirements exist from June to September, as established by the Spanish Technical Building Code (CTE) [33].

The DHW demand is defined according to CTE [34] requirements. In terms of energy, the total yearly demand reaches 1,935 kWh (Figure 3 represents the monthly DHW demand). Due to the instantaneous nature of the DHW consumption and the importance it has on the size of the thermal generator when no DHW accumulation is used, distribution profiles in one-minute time steps were calculated. These profiles were developed through the DHWcalc tool [35],which uses statistical means according to a probability function, defining parameters as the number of draw-off categories for flow rates, or the total daily consumption.

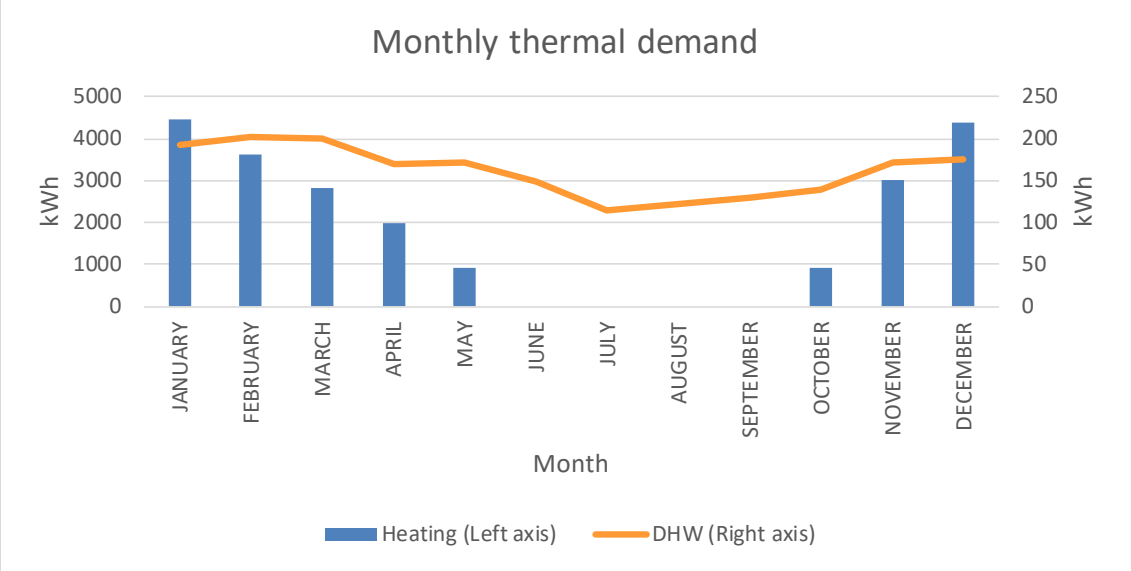

Figure 3. Monthly representation of the annual thermal demands.

Figure 4 and Figure 5 depict the heating and DHW demand for the coldest week in the winter period.

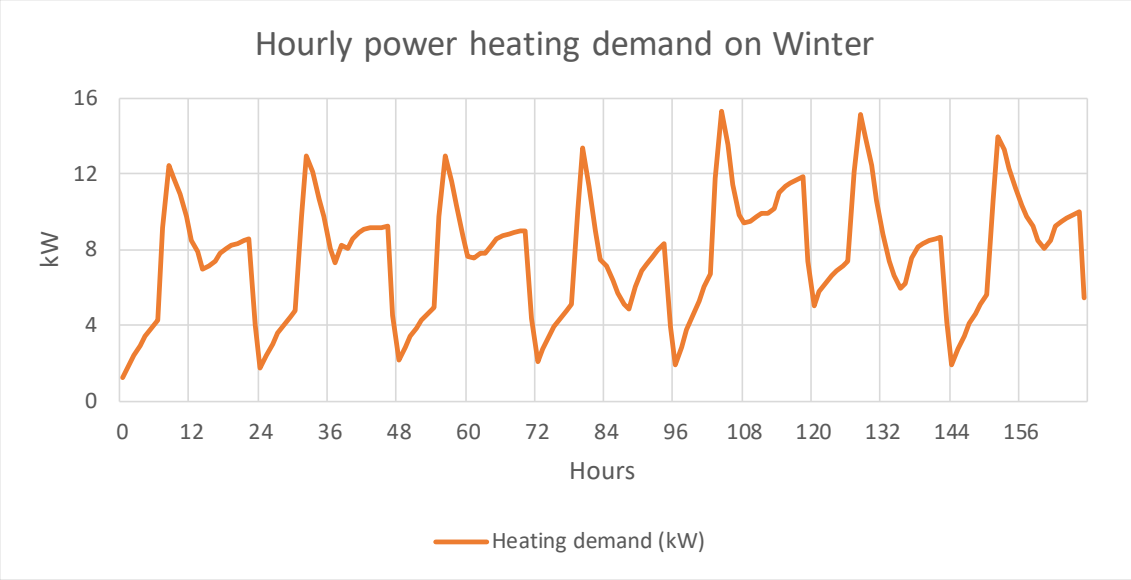

Figure 4. Heating demand for the week with the highest space heating demand.

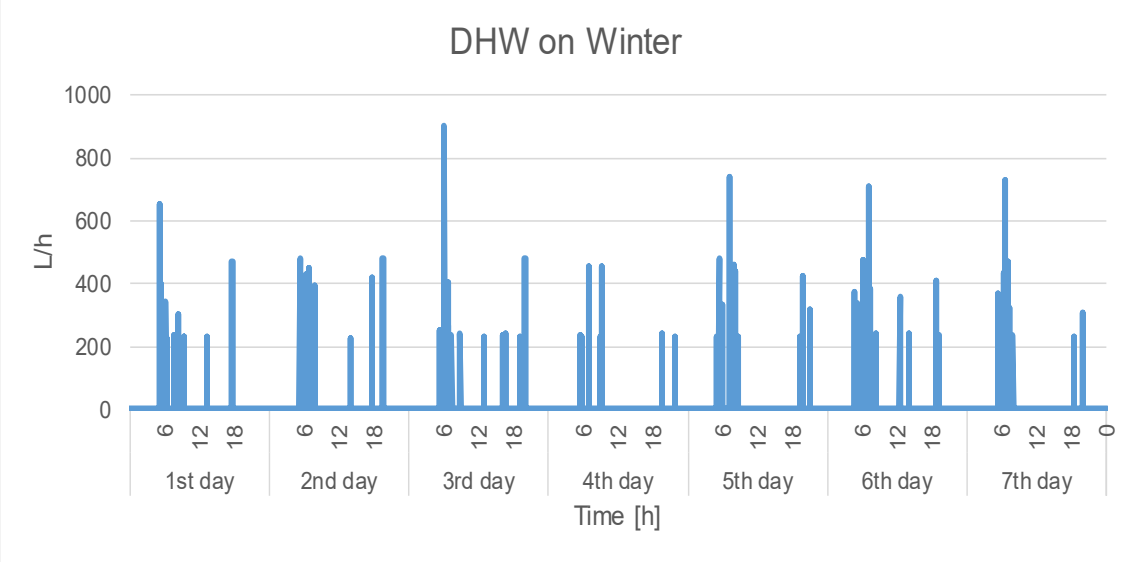

Figure 5. Domestic Hot Water demand for the week with the highest space heating demand.

The equipment installed in the experimental plant was selected to be able to cover the demand curves. The dimensioning of the micro-CHP was carried out following a criterion based on maximizing its contribution to the thermal demand of the final user.

Once the hourly-basis demand for the reference dwelling had been obtained, the annual monotonic heat demand curve was built, as this gives information on the number of hours each demand value is required, as depicted in Figure 6. The design thermal power is obtained by inscribing the rectangle of maximum area in the monotonic heat demand curve [36]. Consequently, a 4.77 kW thermal power value was obtained as the optimum (corresponding to 24.3% of the hourly peak thermal demand), corresponding to 2,170 hours per year running at full load, which turns into covering an energy demand of roughly 10,351 kWh per year; that is, 43% of the yearly heating and DHW demand.

The sizing method can result in a high thermal power and a low number of running hours. To avoid this problem, thermal storage and partial load operation can be used for residential applications. If the SE is able to run at partial load, and it is combined with a TES of 202 L, the SE is able to cover up to 17,314 kWh per year, which corresponds to

72% of the yearly demand. The effect of these combinations is depicted in Figure 6 (b) and (c).

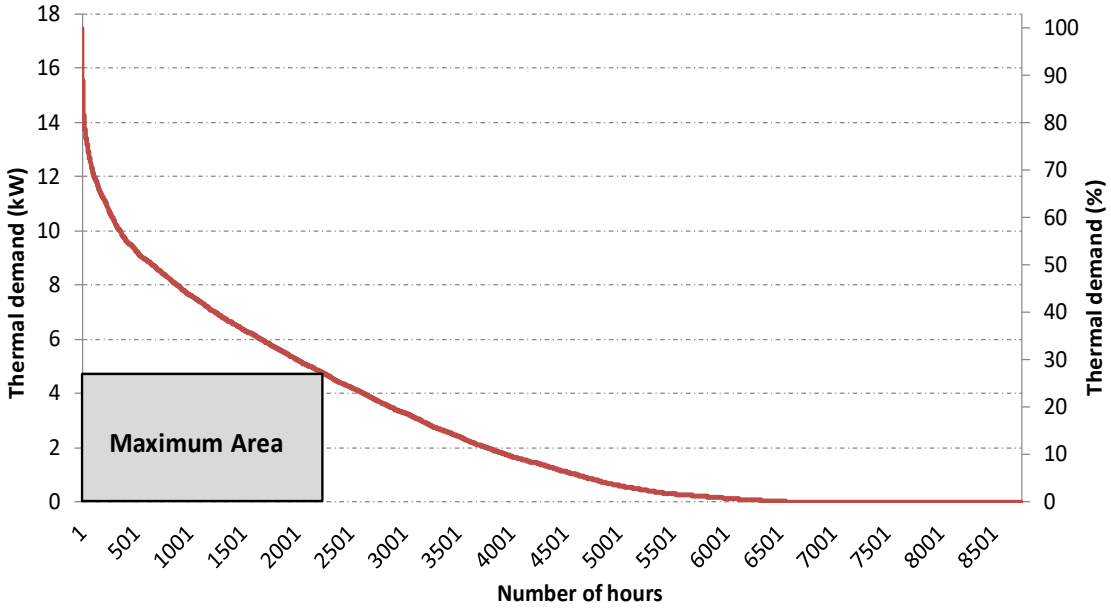

(a)

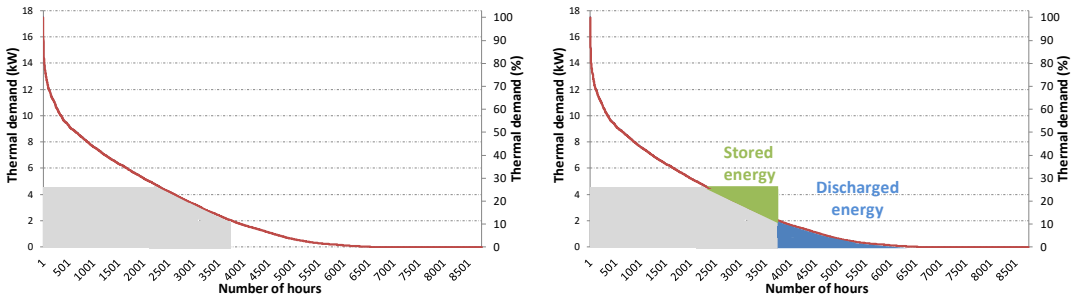

(b) (c)

Figure 6: Maximal area method applied to the monotonic heat demand curve (a) and solutions for incrementing the number of hours of operation: (b) only part-load operation and (c) part-load operation plus energy storage.

Among the commercially available micro-CHP units, the Remeha eVita (around 5 kWt) was chosen as the most appropriate Stirling-based micro-CHP for the case-study and, in more global terms, due to the representativeness of the dwelling assessed, for any detached house in the northern half of Spain. Despite the nominal thermal power being

5 kWt, experimental tests show that this power varies from 4.5 to 5.2 kWt, depending on the return temperature of the cooling water.

2.1.3 Control strategy of the experimental plant

A brief description of the operating mode of the plant is given hereafter and the variables that regulate the control strategy, which are therefore the variables to be optimized, are also explained.

First, it must be pointed out that, even though micro-CHP devices can be controlled either following electricity or heating tracking strategies, in residential uses heating tracking allows the run-time of the micro-CHP to be increased and, in consequence, the useful heat demand-based high efficiency production required by the regulation to be secured[37]. Moreover, the intermittent nature of electric loads in households, together with the fact that these power loads can often be below the minimum electric output of the micro-CHP, makes thermal tracking a better option.

After receiving the thermal tracking-based ON signal of the test, the micro-CHP starts, until it reaches a certain temperature inside the engine (see Figure 1). Then, the impulsion pump, located downstream from the hydraulic compensator where the two generators join, circulates hot water towards the consumption devices, i.e., heating, DHW or both.

If the thermal demand is higher than the SE can supply, then the return temperature (T_{ret_CHP}) to the micro-CHP decreases, which makes it necessary to start the boiler in parallel with the SE. The minimum temperature that makes the boiler work, T_{ret_CHP}, is one of the operational parameters that needs to be optimized.

If the SE can supply the demanded energy by itself, and the return temperature from the consumptions, T_{AVG}, is higher than the storage temperature in the TES, T_{TANK}, the

tank-loading mode begins. The control system compares the difference between both temperatures with two variable set points that have to be optimized: if the temperature difference is greater than ΔT_{charge}^{ON} the load begins, and when it is lower than ΔT_{charge}^{OFF} the tank load ceases.

In the experimental test, when the TES reaches a temperature above 46 ºC, it is considered that there is enough energy to support the SE to cover the demand. If the difference between the temperature of the TES, T_{tank}, and 40 º C is higher than the variable $\Delta T_{discharge}^{ON}$, the TES discharge begins; when it is lower than the $\Delta T_{discharge}^{OFF}$ variable, the discharge stops. These two control variables have also been optimized, always with reference to 40ºC.

2.1.4 Experimental setup and procedures

To conduct the assessment and optimization of this hybrid installation, the plant was operated during the week of highest thermal demand. Since the DHW demand is considerably lower than the heating, and quite similar throughout the year, that week corresponds to January, which is the coldest month at the site where the dwelling is located. With this configuration, the thermal model of the installation was built and further calibrated and validated against the experimental data. Finally, the above-mentioned five operational variables were optimized.

It is also interesting for this research to analyse the effect of the level of the installation's thermal losses. With this aim, the calibrated model of the installation was used to simulate different levels of thermal losses in the installation. The procedure of optimizing the experimental plant was repeated using the same optimization variables for each level of thermal losses.

2.2 Installation modelling

The simulation of the installation was carried out using the commercial software TRNSYS. This is a simulation program for transient systems, which has been widely used and proven effective for the modelling of cogeneration facilities, both in the field of research and engineering [38-40].

The software works with a modular structure, where each component, called Type, models the behaviour of each piece of equipment in the system. Table 2 shows the Types used to define the simulation model of the hybrid system in Figure 1. It can be seen that all the components are taken from the Standard and TESS libraries, except for the micro-CHP. The modelling of this Type has been developed by the authors and is generic and adaptable to most of the SE based micro-CHP units available on the market [41]. It is conceived in terms of a grey-box modelling approach, where all the transitory effects that take place are taken into account. For this purpose, as depicted in Figure 7, two control volumes and a control mass were set out for modelling the dynamic thermal performance of the Stirling engine: the head of the engine (burner) control volume, the engine block control mass and the heat exchanger control volume. All the components are supposed to be thermally defined by a unique mean temperature.

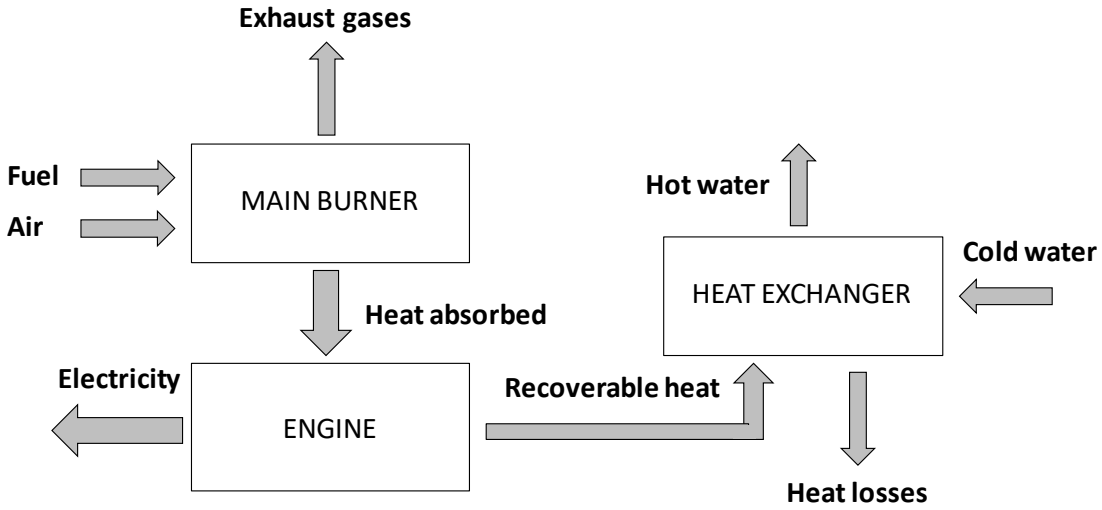

Figure 7: Simplified mass and energy flows of the Stirling micro-CHP model.

Additionally, since the model does not attempt to physically model all the actual phenomena taking place, some considerations were adopted:

- Exhaust gases are replaced by effective heat transfer processes between control volumes.
- Enthalpies of reactants and products are lumped within a combustion efficiency term.
- Fuel is related to the electricity output by means of the electric efficiency.
- Steady-state performance is related to the cooling water temperature and flow through a multiple regression modelling approach.
- A firing rate that reduces the fuel input for part-load operation is defined.
- Independent correlations are used for modelling fuel and electric power during transient phases.

The Type was calibrated and validated against the experimental performance of the tested device. Further information about this Type can be found at [41].

The simulations were carried out during a period of one week, corresponding to the period during which the tests were carried out in the experimental plant. The simulation

time-step was 10 seconds, since this is enough time for the system to take into account the transient heating and cooling processes of the micro-CHP unit, as well as the transient behaviour of the hot water storage tank, as some studies recommend [42].

Table 2. TRNSYS Types used in the simulation

Component	Model	Source
Condensing boiler	Type 700	TESS
Micro-CHP unit	Type 159	Gonzalez Pino [41]
Hot water storage tank	Type 4e	Standard
Hydraulic compensator	Type 4e	Standard
Flow pumps	Type 3b	Standard
Flow diverter	Type 647	Standard
Flow mixer	Type 649	Standard
Differential controller	Type 2b	Standard
Delayed output device	Type 661	TESS
Run-time Calculator	Type 980	TESS
Heat exchanger	Type 91	Standard
Radiator	Type 682b	TESS
Integrator	Type 24	Standard
Periodic Integrator	Type 55	Standard

2.3 Model calibration and validation

Having defined the simulation, but before it can be used to perform the optimization of the experimental plant, it is important to calibrate the model so that the results obtained by the simulation fit the values registered experimentally. In this research, a two-step calibration is performed, as this has proven to be effective in some studies [43, 44]. In the first step, the experimental plant model was calibrated using the instantaneous outlet temperature of the boiler and the SE, as well as their fuel consumption. In the second, the model was calibrated to better adjust to the total quantity of heat discharged from storage and the total fuel consumption of the boiler. The highest thermal demand week was simulated, using the first 48 hours to perform the calibration. The model was then validated, assessing its performance over the whole week.

A deterministic calibration method was chosen to minimize the discrepancies between the simulation and the experimental plant. This is based on the application of an optimization algorithm that varies a series of parameter values until the cost function,

which quantifies the difference between simulation and reality, is minimized. The software GenOpt 3.0.1 [45] was used to perform the calibration, applying the GPS Hooke-Jeeves algorithm to select the parameter values for the successive iterations of the calibration process. This calibration methodology was thoroughly explained in [46].

The Coefficient of Variation of the Root Mean Square Error CV (RMSE), as defined by equation (1), determines the differences between the simulation results and the experimental data. For the first step of calibration, the results compared to verify the accuracy of the simulation are the impulsion temperatures of the generation devices (boiler and Stirling) and, their fuel consumption. Therefore, the minimized cost function in the calibration is obtained through equation (2), as the mean of the CV (RMSE) of each variable.

$$CV\ (RMSE) = {RMSE}/{\bar{X}_{real}} = {(\sqrt{\sum_{i=1}^{n}(X_{sim} - X_{real})^2}/n)}/{\bar{X}_{real}}, \quad (1)$$

$$CV\ (RMSE)_{step\ 1} = {(CV(RMSE)_{T_{CHP}} + CV(RMSE)_{T_{BOI}} + CV(RMSE)_{F_{CHP}} + CV(RMSE)_{F_{BOI}})}/{4}. \quad (2)$$

where:

- X_{sim} is the simulated value.
- X_{real} is the measured value.
- $\overline{X_{real}}$ is the average measured value.
- n is the number of data points.
- T_{CHP} is the impulsion temperature of the micro-CHP [ºC].
- T_{BOI} is the impulsion temperature of the boiler [ºC].
- F_{CHP} is the fuel consumption of the micro-CHP in each time step [kWh_{LHV}].
- F_{BOI} is the fuel consumption of the boiler in each time step [kWh_{LHV}].

For the second step calibration, the cost function also considers the total quantity of heat discharged from storage (STO) in [kWh] and the total fuel consumption of the boiler (F_{BOI_tot}) in [kWh$_{LHV}$], as shown in equation (3).

$$CV\ (RMSE)_{total} = \begin{matrix}(CV(RMSE)_{T_{CHP}} + CV(RMSE)_{T_{BOI}} + CV(RMSE)_{F_{CHP}} + \\ CV(RMSE)_{F_{BOI}} + CV(RMSE)_{STO} + CV(RMSE)_{F_{BOI\_tot}})/6\end{matrix} \quad (3)$$

The parameters used to calibrate the model were chosen after performing a global sensitivity analysis based on a screening method. A parameter screening is a mathematical method that allows a quantitative classification of the input parameters defining a computational model, in order of their influence in the simulation output. The elementary effects method, proposed by Morris [47], is used and a set of 18 initial parameters is assessed.

After performing the parameter screening, seven parameters were identified as the most influential in the simulation; so they were the ones chosen for the first step calibration. In the results section, Table 5 shows the parameters and their initial and calibrated values.

Subsequently, for the second step, the heat loss coefficients from the Hydraulic Compensator and the TES system were calibrated. Although these parameters do not appear as the most important ones in the sensitivity analysis, they significantly affect the total gas consumption. The initial and final values of these parameters are also included in Table 5.

2.4 Optimization

The optimization is carried out by a multi-objective approach in which all the objective functions are considered simultaneously. The methodology followed to apply the optimization of the calibrated model of the installation is described hereafter.

2.4.1 Objective function and optimization variables

The hybrid micro-CHP plant was optimized taking into consideration two different criteria that quantify the economic and exergy performance of the facility. From the economic point of view, the objective was determined through equation (4), minimizing the operational cost of the plant in the time horizon of the test corresponding to one week.

$$\min Cost = \sum_{t=0}^{10080} ((F_{CHP} + F_{BOI}) \cdot c_F) - \sum_{t=0}^{10080} (E_{CHP} \cdot c_E) \quad (4)$$

where F_{CHP} and F_{BOI} are the fuel consumption in each time step in [kWh$_{LHV}$], E_{CHP} is the electricity generated in each time step by the micro-CHP in [kWh], and c_F and c_E are the costs of natural gas and electricity, respectively, in [€/kWh$_{LHV}$].

The second objective function maximizes the overall exergy performance of the installation. Equation (5) presents the calculation of the exergy efficiency, where the products obtained are the exergy used for heating (dissipated in the fan coil) and the DHW production and the electricity generated in the SE, for which the exergy of the fuel used by both the micro-CHP and the boiler devices was consumed. It is necessary to transform the maximization function of the exergy into a minimization function, as calculated by equation (6), so it can be included in the optimization algorithms.

$$\max \psi = \sum_{t=0}^{10080} \left(E_{CHP} + Ex_{Heating} + Ex_{DHW}\right) \Big/ \sum_{t=0}^{10080} \left((F_{CHP} + F_{BOI}) \cdot r_{ex-e}\right) \quad (5)$$

$$\max \psi = \min(1 - \psi) \quad (6)$$

The exergy used for heating ($Ex_{Heating}$) and DHW production (Ex_{DHW}) in each time step [in kWh] was calculated according to the general equation of the exergy of a water flow, indicated in equation (7), where T_0, T_1, T_2 are the environment, the inlet and the outlet temperatures, respectively, in [K] of an $\dot{m}$ mass flow rate with a c specific heat. The

exergy of the fuel consumed was obtained by the exergy-energy ratio for the LHV of the natural gas ($r_{ex-e} = 1.04$).

$$Ex = \dot{m} \cdot c \cdot \left(T_2 - T_1 - T_0 \cdot \ln\frac{T_2}{T_1}\right) \quad (7)$$

The environmental criterion, which seeks to minimize the GHG emissions, was not analysed here, since it was considered that the configuration that minimizes costs also minimizes CO_2 emissions, as both economic and environmental objectives only differ in the ratios of cost and emissions of electricity and natural gas.

The variables that define the operating mode of the plant influence the thermodynamic and economic behaviour of the system. Therefore, the optimization of the micro-CHP installation is performed by determining the proper operating values for those variables. Table 3 presents the variation range of the set point of the five variables assessed, which were explained above in 2.1.3.

Table 3. Optimization variables limit values.

Variable	Units	Min. value	Max. value
T_{ret_CHP}	°C	30	50
ΔT^{ON}_{charge}	°C	0	20
ΔT^{OFF}_{charge}	°C	0	10
$\Delta T^{ON}_{discharge}$	°C	0	20
$\Delta T^{OFF}_{discharge}$	°C	0	10

2.4.2 Multi-objective optimization with GA

The GA for problem optimization are based on Darwin's theory of evolution and the idea that nature selects the optimal choice [48]. The application of a GA starts with the coding of the problem variables as chromosomes, represented by strings of binary digits, and the random selection of the initial population, called parent population. At each iteration, the aptitude of the population is evaluated and only the most qualified individuals are chosen for reproduction. An offspring generation is obtained by

reproduction of the parent population, through GA operators: selection, crossover and mutation. The iterations continue until the stop criterion is reached, which can be a maximum number of iterations or convergence, when the changes in the population are lower than a fixed level.

Based on the objectives previously set out, the optimization problem is that defined by equation (8):

$$minimize \begin{cases} f_1(x) = Cost \\ f_2(x) = (1 - \psi) \end{cases} \quad (8)$$

The algorithm used here to perform the multi-objective optimization is NSGA-II. Deb et al. [22] explain that it amends GA problems due to the computing complexity, the non-elitism approach and the need to specify a sharing parameter. The algorithm is improved by introducing a fast non-dominated sorting procedure with an elitist-preserving approach and a niching operator with no parameters. The non-dominated criterion ranks population members, the elite preservation mechanism enhances convergence to the Pareto-optimal front and the crowding distance preserves the diversity of solutions by choosing solutions in less crowded regions.

For the application of the NSGA-II method to this work, the tool JEplus + EA [49] was used, as it has been proven a valid tool to solve multi-objective optimization problems together with building performance simulation software, as in [50]. This tool is prepared to define parametric runs so the successive TRNSYS samples can be automatically executed in parallel. It simultaneously collects the results obtained in each simulation and applies the NSGA-II algorithm to perform the process of evaluation and generation of populations in the evolutionary process of optimization. Figure 8 presents the joint operational diagram of the simulation software and the optimization tool.

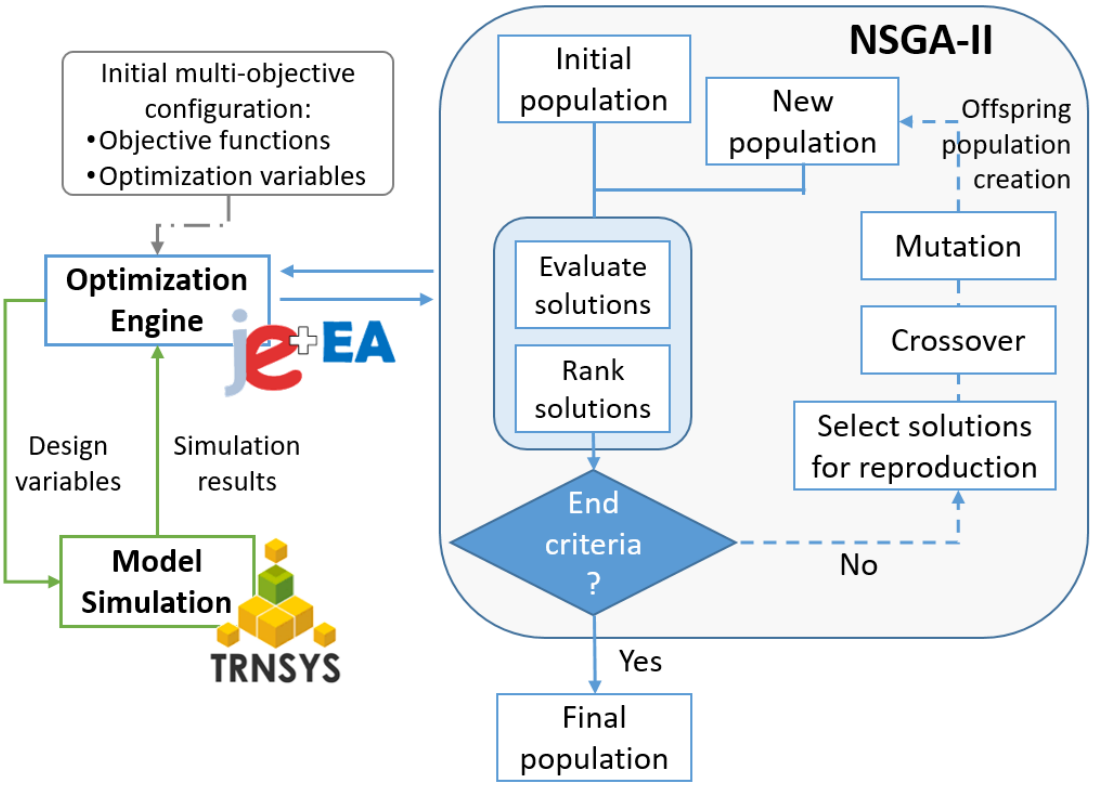

Figure 8. Flowchart diagram of the multi-objective optimization process.

The optimizer parameters that define the algorithm are presented in Table 4. The population size is selected following the recommendation to be twice or four times the number of input variables [51]. Although the number of generations suggested is lower, in this study, 100 generations are evaluated so as to ensure that global optimal solutions are reached. Crossover and mutation rates are chosen based on the statistical analysis of 68 optimization related research articles [52].

Table 4. NSGA-II optimizer parameter values

NSGA-II parameter	Value	Description
Population size	20	number of solutions to be evaluated in each iteration
Maximum number of Generations	100	number of iterations to be run in the optimization
Crossover rate	0.9	frequency of merging features of existing solutions
Mutation probability rate	0.355	frequency of random changes
Tournament size	2	number of solutions randomly selected to be compared by their fitness value

In a multi-objective problem, there is no single optimal solution, but a set of solutions that best satisfy the different objectives. This set of optimal solutions is known as the Pareto-frontier and includes those solutions that are dominant with respect to the others. A solution is Pareto-optimal if one of its objectives cannot be improved without worsening any of the others, i.e., it is a non-dominated solution.

There are several criteria to select the best point in the Pareto-frontier, e.g., based on the decision makers' experience in choosing the most suitable for their own requirements, weighting the different objectives according to importance indicators, or identifying the point with the minimum distance to the ideal point. The decision-making method applied in this research is the last named, as it has been successfully used to determine the best solution in other multi-objective problems [19, 53].

It is usually convenient to normalize the objectives in order to facilitate the comparison between different objectives, as proposed in [19]. Each of the studied objectives are normalized following equation (9).

$$x^* = (x - x_{min})/(x_{max} - x_{min}), \tag{9}$$

where x^* represents the normalized value of the objective x. Thus, x^*, y^* are the normalized values of the objectives x, y defined according to equations (4) and (6).

Then, the so-called ideal point is determined, which is the solution that would suppose the minimum value for each objective, a point impossible to reach. By means of equation (10), the distance between the ideal point and every Pareto-optimal solution is calculated, so the one with the minimum value for that distance is accepted as the optimum.

$$d = \sqrt{x^{*2} + y^{*2}} \tag{10}$$

3 Results and discussion

In this section, the experimental results of the installation during the analysed period of maximum thermal demand in the dwelling are presented. Subsequently, the calibration and validation of the model of the installation are shown. Thirdly, the optimizations results are included, and finally, the global variances in the operation of the experimental plant for the different operational modes are discussed and compared.

3.1 Experimental results

The results of the experimental test are shown in Figure 9 and Figure 10. More specifically, the corresponding results are from a specific day of the test, so they can be seen more clearly.

Figure 9(a) shows the different productions and consumptions of the boiler and SE for the fifth day, the one with the highest demand of the week. As stated in section 2.1.3, the SE and the condensing boiler operate in parallel if the T_{ret_CHP} is lower than 40 ºC (see Figure 9(b)).

Another important aspect of the experimental tests is how the installation operates during TES charge and discharge periods. With the objective of showing this mode of operation, Figure 10 is shown in two parts.

Figure 10(a) shows the conditions of discharge: The control strategy established so that, when the temperature of the TES is higher than 46 ºC, the discharge begins and the heat from storage is negative. This operation mode continues until the temperature of the tank is lower than 40 ºC.

In Figure 10(b), the conditions of charge periods are also shown. The charge only happens if the difference between the temperature T_{AVG} (see Figure 1) and the TES temperature (T_{TANK}) is higher than 2ºC. This process continues until this difference is

lower than 0ºC. It can be seen that some small discharges occur when the conditions for discharge do not exist. This is because, when there is a change in the mode of operation, it takes a little time until the valve closes and, in that period of time, the heat quantity is negative.

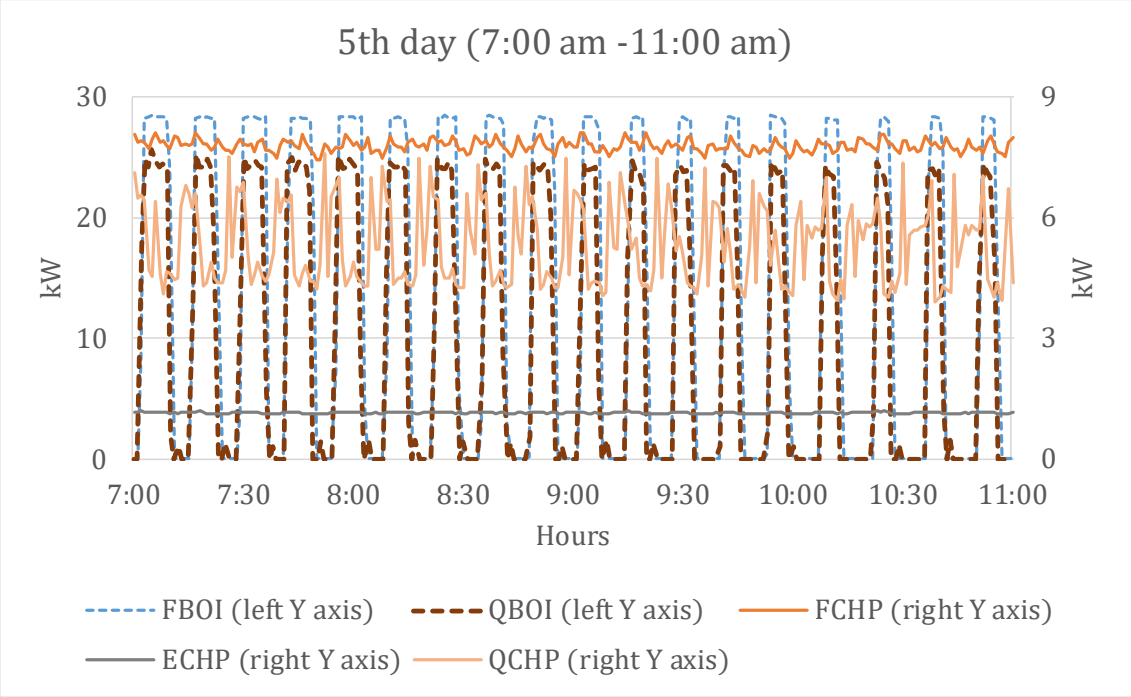

(a)

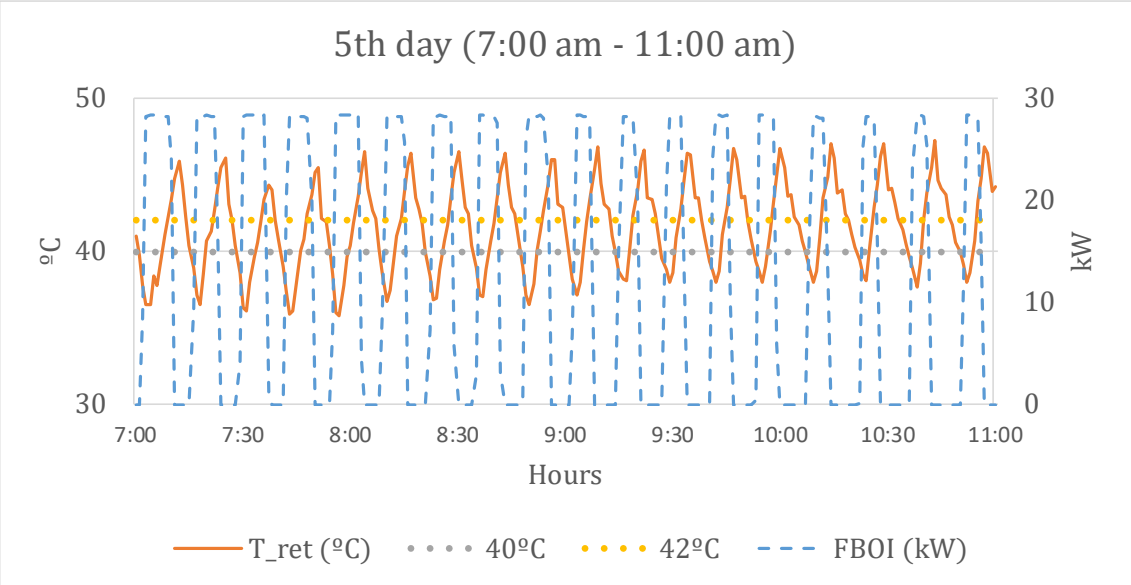

(b)

Figure 9. Boiler and micro-CHP working together from 7am to 11am during the 5th day. (a) Fuel consumption and production. (b) Boiler's ON/OFF cycles.

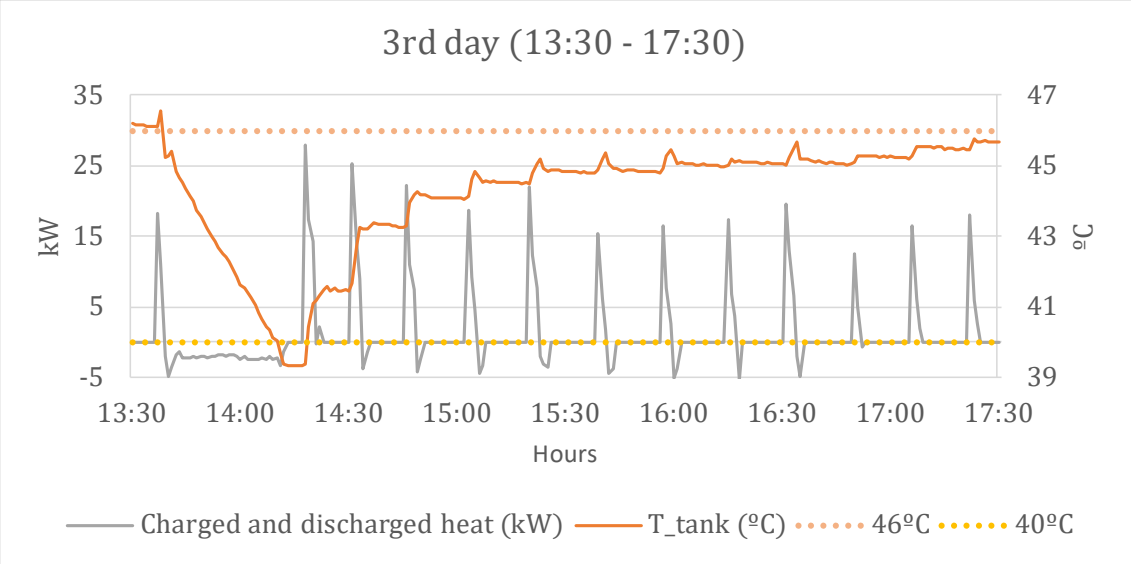

(a)

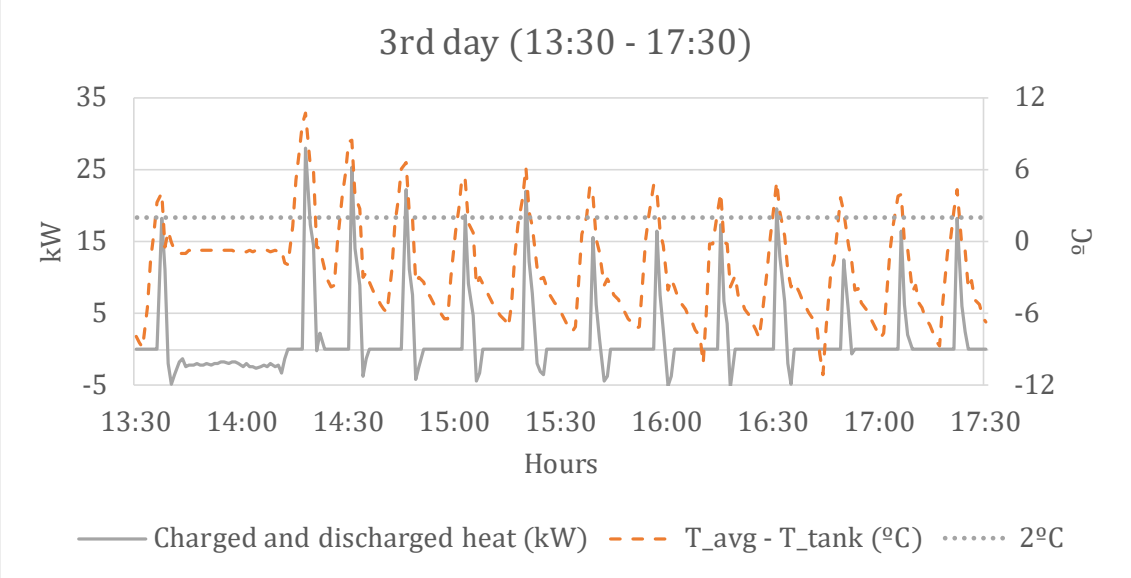

(b)

Figure 10. (a) Conditions of discharge combined with the heat from storage. (b) Conditions of charge combined with the heat from storage.

3.2 Calibration results

The TRNSYS model was calibrated using GenOpt, obtaining the minimum of the objective function for the first step of calibration, defined in equation (2), after 248 iterations performed in a PC with an INTEL CORE I7 processor and 32 gigabytes of RAM. Table 5 shows the parameters used to calibrate the TRNSYS model, including their

initial values, the possible range of variation, and their final values once the model has been calibrated. The first seven are from the first step of calibration and the last two from the second step.

Table 5. Identification and value ranges of the calibration parameters.

1st step calibration					
Name	**Units**	**Inf. Limit**	**Sup. Limit**	**Initial value**	**Calibrated value**
Boiler rated capacity	W	25,350	28,020	26,700	26,700
Flow rate of the boiler pump	kg/s	0.28	0.31	0.29	0.30
HC volume	m^3	0.02	0.5	0.05	0.12
TES volume	m^3	0.1	1	0.2	0.2
LHV of the natural gas	Wh/kg	10,480	15,710	13,100	13,090
Micro-CHP rated gas mass flow rate	kg/s	1.04E-04	1.57E-04	1.31E-04	1.31E-04
Flow rate of micro-CHP pump	kg/s	0.09	0.21	0.14	0.12
2nd step calibration					
Name	**Units**	**Inf. Limit**	**Sup. Limit**	**Initial value**	**Calibrated value**
HC heat loss coefficient	W/K	0.2	4.75	0.43	1.52
TES heat loss coefficient	W/K	25.8	120.6	31.0	74.96

When analysing Table 5, the initial and calibrated values of the first step seem very similar, even though their effect on the improvement of the dynamic answer on the boiler operation is important. Figure 11 graphically verifies that the first step calibrated model is able to follow the real experimental dynamics. Likewise, Figure 12 displays the improvement of the dynamics in the fuel consumption of both pieces of equipment, comparing the initial model and the first step calibrated model results with the real ones. Therefore, since the initial and calibrated values of the first step are similar (see Table 5), Table 6 shows that the initial model had already reduced simulation errors and the improvement in the dynamics just represents a decrease in the total CV (RMSE) of 12.23%.

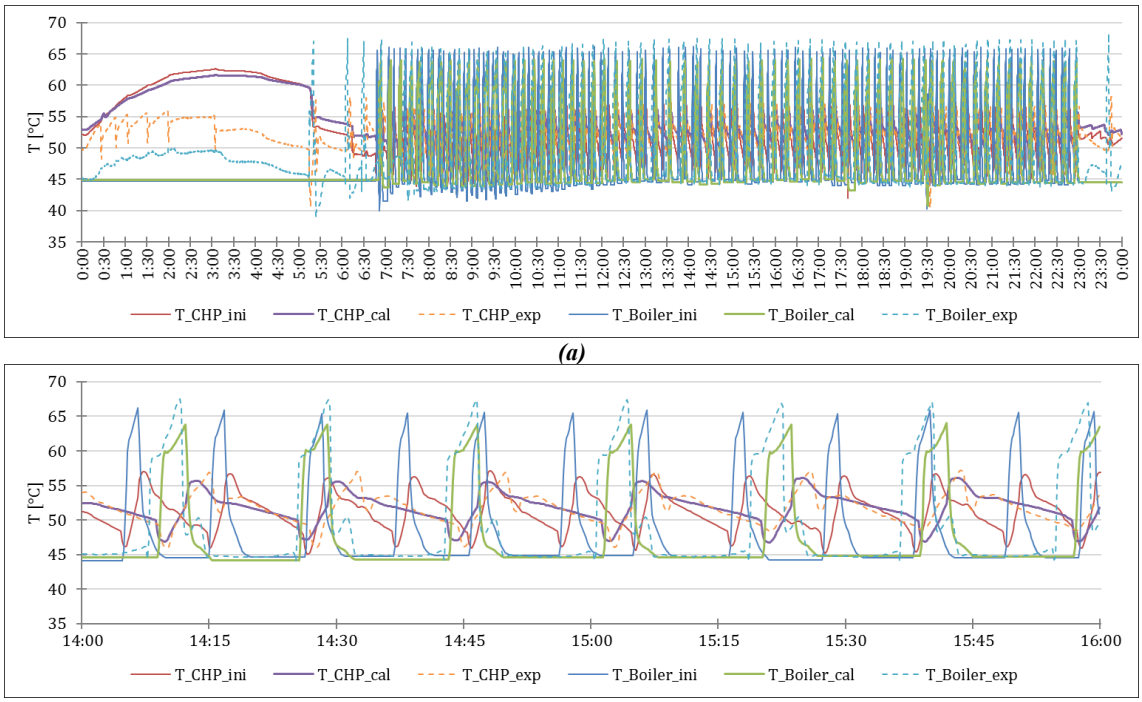

(a)

(b)

Figure 11. Outlet temperature of the micro-CHP and boiler: simulated before (ini) and after first step calibration (cal) and experimental values (exp). (a) 24-hour period and (b) 2-hour period.

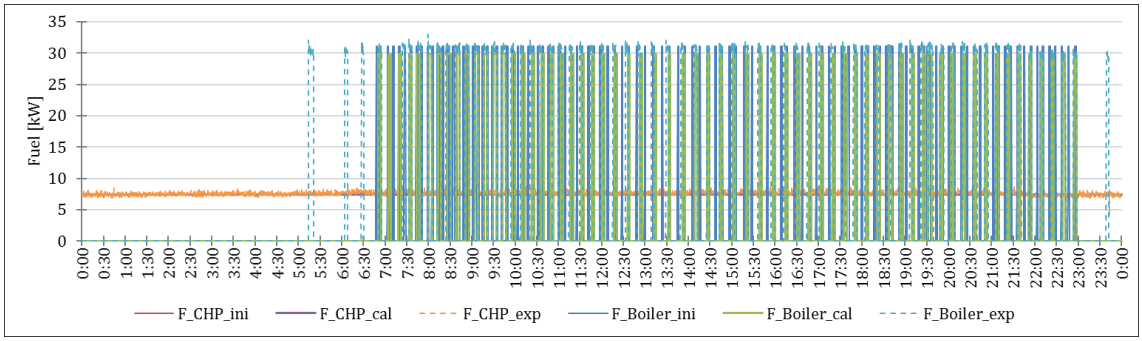

(a)

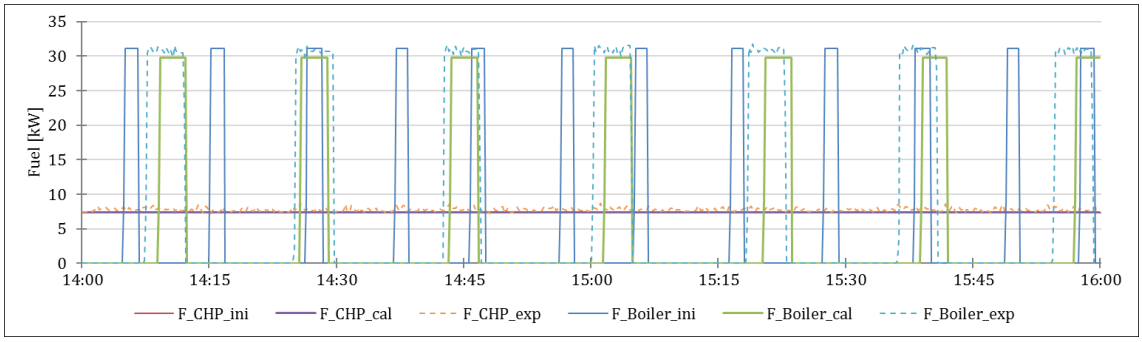

(b)

Figure 12. Fuel consumption of the micro-CHP and Boiler: simulated before (ini) and after calibration (cal) and experimental values (exp). (a) 24-hour period and (b) 2-hour period.

Table 6. Statistical error indices of the initial and first step calibrated model.

	RMSE				CV(RMSE)
	T_{CHP}	T_{BOI}	F_{CHP}	F_{BOI}	Total
Initial	1.91E-02	2.32E-02	1.41E-03	6.87E-02	8.76E-04
Calibrated	1.43E-02	2.02E-02	1.43E-03	6.10E-02	7.69E-04
Reduction (%)	25.18%	13.04%	-1.49%	11.19%	12.23%

For the first step calibrated model, the results of total consumption at the boiler and the total discharged heat from storage are 21% and 41%, respectively, lower than the experimental results (see Table 7). To reduce this gap, the second step calibration is performed, where the parameters studied are the transmission losses that exist in the experimental installation through the heat loss coefficients of the TES and the HC, whose initial values and calibrated values appear in Table 5.

The calibrated values are close to the real operational ones obtained from the experimental data, which are 68.3 and 2.1 W/K for the TES and the HC, respectively. Note that the TES heat loss coefficient also considers all the circuit losses from the HC to the TES, while the HC heat loss coefficient also considers the circuit losses from the HC to the generation devices. The cost function for this step is equation (3). Table 7 shows the results of the final calibrated model contrasted with the experimental and first step calibration results.

Table 8 presents the second step calibration statistical indices, including those for the total fuel consumption at the boiler and the heat used from storage. Although, individually, some of the error indices grow (negative ones), the total CV(RMSE) is reduced by 57.6% from the initial simulation.

Table 7: Experimental results versus the first and second step calibrations.

	EXPERIMENTAL TEST	SIMULATION	
		First step Calibration	Second step Calibration
Micro-CHP fuel consumption (kWh_{LHV})	1,285.9	1,229.4	1,234.5
Boiler fuel consumption (kWh_{LHV})	1,108.5	870.2	1,144.9
Total of fuel (kWh_{LHV})	2,394.4	2,099.6	2,379.4
Heat Production CHP (kWh)	880.9	810.6	817.5
Electric Production CHP (kWh)	191.6	187.7	188.9
Thermal Efficiency of CHP	68.50%	65.90%	66.22%
Electric Efficiency of CHP	14.90%	15.27%	15.30%
Heat Production Boiler	849.0	665.0	875.0
Thermal efficiency of Boiler	76.59%	76.41%	76.43%
Heat losses (transmission + Fumes) (kWh)	890.9	790.8	881.8
Heat supplied for DHW(kWh)	20.7	20.8	21.5
Heat supplied for Heating (kWh)	1291.2	1,287.9	1287.3
Total energy discharged from TES (kWh)	13.6	7.9	13.5
Global Energy Efficiency	62.79%	71.27%	62.94%
Global Exergy Efficiency	13.33%	15.00%	13.29%
Hours of CHP in operation	168	168	168
ON/OFF cycles of Boiler	486	470	610
CO_2 emissions (kg)	435.8	382.1	433.1

Table 8: Statistical error indices of the uncalibrated initial model and 2nd step calibrated model.

	RMSE						CV(RMSE)
	T_{CHP}	T_{BOI}	F_{CHP}	F_{BOI}	STO	F_{BTOT}	Total
Initial	1.91E-02	2.32E-02	1.41E-03	6.87E-02	5.15E+00	2.53E+02	1.59E-01
Calibrated	1.48E-02	2.61E-02	1.43E-03	7.16E-02	1.88E-01	3.64E+01	6.76E-02
Reduction (%)	22.62%	-12.58%	-1.49%	-4.21%	96.6%	85.60%	57.60%

Analysing Table 7, it can clearly be seen that the total consumption at the boiler and the total discharged heat from storage for the second step calibrated model fit the experimental results properly. During this second step calibration, where the heat losses of the model have been adjusted to the reality, there is only one parameter that has worse behaviour than the first step calibration when compared to the experimental results. The on/off cycles of the boiler have increased from 470 to 610. The two step calibration is necessary because, in the first step, the model has been calibrated against instantaneous variables (T_{CHP}, T_{BOI}, F_{CHP}, F_{BOI}), while in the second step, the totalized variables have

been calibrated (STO, F_{BTOT}). Thus, the first step calibration focused on the detailed dynamics of the system, while the second focused on global performance parameters. As the global performance is more important for this optimization work, the order of calibration has been first the dynamics followed by the global parameters. Note that the calibration procedure mixing global parameters and instantaneous parameters has given worse results.

3.3 Multi-objective optimization results

After the application of the NSGA-II algorithm for the multi-objective optimization of the modelled plant, the Pareto frontier, represented in Figure 13, is obtained. Here, it is important to recall that the objective depicted in the Y axis is the one presented in equation (6), to transform the maximization of the exergy performance into a minimization objective. In Figure 13, the cost and thermodynamic optimized points are shown, which are the best individual points for the considered objectives.

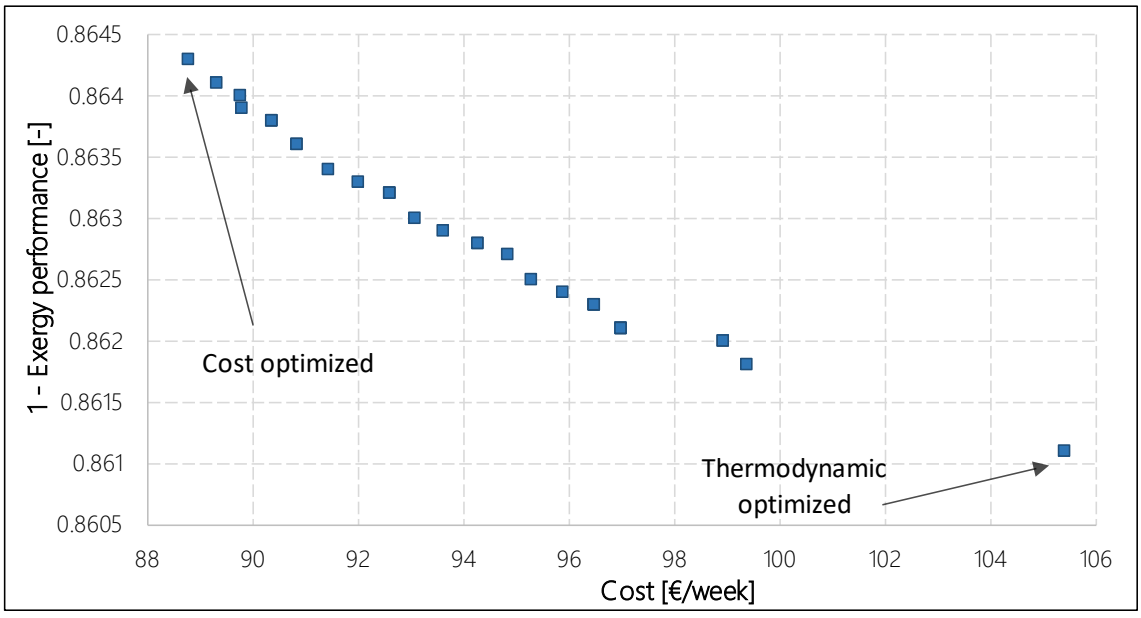

Figure 13. Pareto frontier.

The Pareto frontier is normalized, obtaining a new curve, which is represented in Figure 14. The distance to the ideal point is calculated according to equation (10). This

distance d is also depicted in Figure 14, and the point with the minimum distance is indicated.

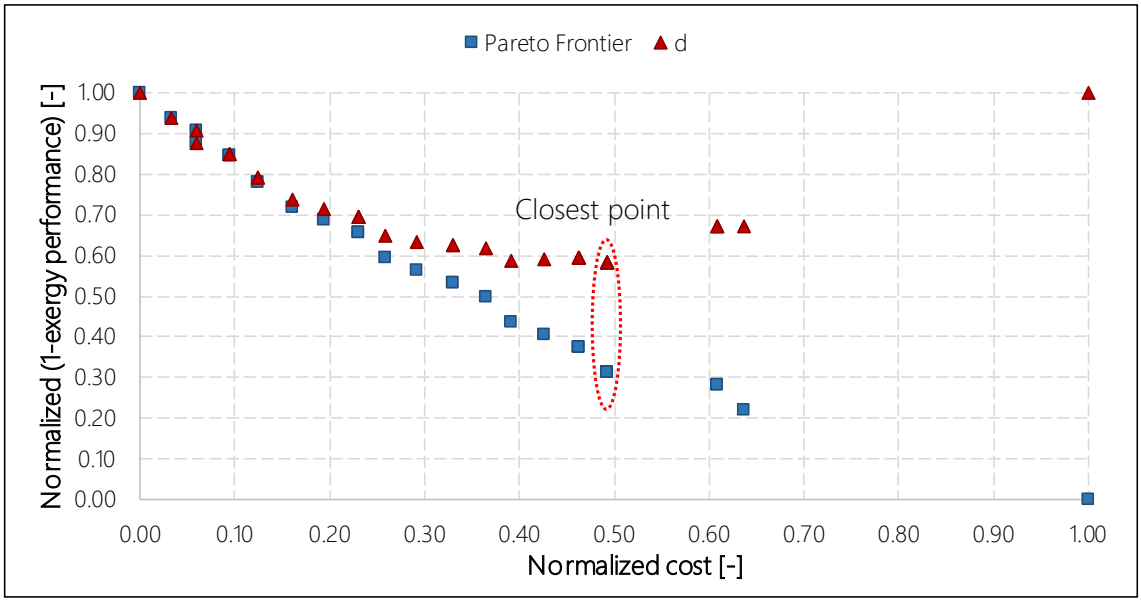

Figure 14. Pareto frontier of the normalized objectives and distance to the ideal point.

Table 9 shows the values of the cost and exergy performance, together with the normalized cost and [1 – exergy performance] calculated using Equation 9 for the main scenarios. The most significant values of the Pareto curve are presented for the experimental case, the cost optimized scenario, the multi-objective optimized scenario and, finally, the exergy optimized scenario.

Table 9: Summary of the cost and exergy efficiency for the main scenarios considered in the Pareto curve.

Optimization scenario	Cost [€/week]	Exergy efficiency (%)	Normalized cost	Normalized [1-exergy performance]
Experiment case	104.31	13.29	-	-
Cost optimized	88.79	13.57	1.00	0.00
Multi-objective optimized	96.99	13.79	0.49	0.31
Exergy optimized	105.42	13.89	0.00	1.00

The results achieved for the five optimization variables with different scenarios, according to the level of thermal losses, are shown in Table 10. These levels of thermal losses were established to reduce the experimentally measured transmission losses of the

installation, which are 17% of the LHV fuel consumption, so the proposed levels are the ones that reduce these losses to 15%, 10%, 5% and 0%.

Table 10. Values of the optimization variables before and after the optimization process.

Variable	Non-optimized	Optimized 17% losses	Optimized 15% losses	Optimized 10% losses	Optimized 5% losses	Optimized 0% losses
T_{ret_CHP}	40	37.5	35	36.5	36	47.5
ΔT_{charge}^{ON}	2	20	20	20	18.6	12
ΔT_{charge}^{OFF}	0	10	10	10	10	9.2
$\Delta T_{discharge}^{ON}$	6	1.8	1.8	0.8	0.4	0.8
$\Delta T_{discharge}^{OFF}$	0	1.2	1	0.6	0.2	0

Table 10 shows that the temperature at which the boiler is switched ON is reduced from the experimental value in each case, except for the ideal case of 0% transmission losses. This reduction is because one of the optimization objectives is the reduction of the operational cost, thus the minimization of fuel consumption. Establishing a lower temperature to switch ON means that the boiler operates for less time, so a reduction in the operational cost is obtained. Thanks to the better insulation and lower thermal storage use, the lower thermal losses obtained permit the required demand to be supplied with a lower boiler use. For the ideal 0% transmission losses case, the optimized case storage use increases drastically and thus, to reduce the boiler consumption while it increases the storage use, a higher T_{ret_CHP} set point to switch ON the boiler is needed.

The temperatures that allow the charging of the TES are higher when compared with the non-optimized set points. This increment makes it difficult to start the charge, so the quantity of heat charged decreases from the experimental case. Furthermore, this effect lowers the weekly average tank temperature to the range of 30ºC to 35ºC, thus reducing the thermal losses of the TES. The tank is now mainly charged during low demand periods at night when the CHP heat power exceeds the demand and is then completely discharged in the early morning hours when the demand increases. For the

0% losses case, the set point to charge the storage is reduced, while the set point to switch ON the boiler increases, also making the storage use more frequent during daytime operation.

The set point temperatures that switch ON the discharge of the TES are lower than the experimental values in order to facilitate this operation mode. In reality, during the night hours, when the thermal demand is lower than the CHP heat production, since the circuit temperature increases, even though discharge conditions exist, the inlet temperature to the TES is higher than the TES temperature. Thus, during the nights, the optimized discharge conditions are actually making it possible to heat up the TES, to as high as 57ºC, reaching the CHP OFF signal temperature. Thus, although the optimized discharge set points presented in Table 10 seem to be illogical, it is the mechanism used by the optimization program to permit the charging of the TES system during the night to much higher temperatures than those permitted by the optimized charge set points in Table 10. Basically, the optimization is generating very strict charge conditions that are effective during high demand hours and uses the discharge conditions to heat up the TES during low thermal demand hours at night. The use of discharge conditions for charging the TES during the low demand hours should be studied in detail and will probably lead to a general control logic redefinition.

Finally, to show what the improvements in the installation are if these control variables were changed, attention must be paid to the objectives explained before, which are the exergy efficiency and the cost. In each case, the improvement presented is calculated with respect to the non-optimized values.

For the real case, in Table 11, it can be seen that a reduction of 7.01% in cost is achieved. According to exergy, the exergy efficiency optimization results are presented

as defined by equation (5). As can be seen, in the experimental case, an increase of 3.91% in exergy efficiency can be obtained by optimizing the control variables.

Table 11. (a) Results of the optimization objectives before and after the optimization process for the real case. (b) Results of the optimization objectives before and after the optimization process for different levels of thermal losses.

Objective		Non-optimized	Optimized
COST		104.31	96.99
	reduction	--	7.01 %
EXERGY		13.29 %	13.81 %
	increase	--	3.91 %

(a)

Objective		Non-optimized 15% losses	Optimized 15% losses	Non-optimized 10% losses	Optimized 10% losses
COST		102.92	92.48	93.77	88.81
	reduction	--	10.14 %	--	5.29 %
EXERGY		13.59 %	13.95 %	14.42 %	14.66 %
	increase	--	2.65 %	--	1.66 %
Objective		Non-optimized 5% losses	Optimized 5% losses	Non-optimized 0% losses	Optimized 0% losses
COST		86.47	83.25	78.86	78.84
	reduction	--	3.72 %	--	0.03 %
EXERGY		15.38 %	15.41 %	16.38 %	16.85 %
	increase	--	0.19 %	--	2.87%

(b)

Table 11 permits an interesting trend to be obtained on the optimized cost reduction potential, while the level of energy losses decreases. Assuming an adiabatic circuit and TES system, the cost reduction is 0% if the nonoptimized and optimized cases are compared. This is logical, since the energy losses are zero and thus, independently of the control strategy used, the supplied energy will be the same for the heating and DHW system. During the analysed week, the Stirling engine was working non-stop for all the cases, except for the adiabatic optimized case, where the engine works 167 hours instead of 168. This leads to the conclusion that the cost reduction (and thus the energy consumption) will not be dependent on the control strategies applied to this case. Then, the cost or energy optimizations of research works that optimize adiabatic models of hybrid systems are insensitive to the selected control variables. Furthermore, the latter is

extensible to models which consider that the heat losses occur within the building thermal envelope as useful heat.

This is not the case for the exergy efficiency, since even for the adiabatic case, there is some margin of improvement due to the use of storage. For the adiabatic case, the optimized system aims to maximize the use of the TES to avoid the use of the boiler and thus maximize the exergy efficiency by generating electricity through the SE.

3.4 Optimized scenarios

This section presents a summary of the main indicators of the behaviour of the installation for different scenarios: the experimental test is compared to the results of the simulations for the non-optimized model and the optimized one. Table 12 shows the operation for the real experiment, where the heat losses are 17%. Then, Table 13 shows the results for the optimized cases, where the transmission losses are 15%, 10%, 5% and 0% with the optimization of each case.

On the one hand, if the results of different levels of thermal losses in the non-optimized scenarios are compared, it is clear that the consumption of fuel at the boiler decreases due to fewer ON/OFF cycles in this device. The reduction of the thermal losses in the installation has, as a result, a lower cooling of the water, so the inlet temperature to the SE is lower than T_{ret_CHP} less often. Since the boiler has fewer ON/OFF cycles, the destruction of exergy is lower, so the exergy efficiency grows.

Table 12. Experimental test and simulation pre-optimized and optimized results.

	EXPERIMENTAL TEST	SIMULATION (17% LOSSES)	
		NON OPTIMIZED	OPTIMIZED
Micro-CHP fuel consumption (kWh_{LHV})	1,285.9	1,234.5	1,234.5
Boiler fuel consumption (kWh_{LHV})	1,108.5	1,144.9	1,009.6
Total of fuel (kWh_{LHV})	2,394.4	2,379.4	2,244.0
Heat Production CHP (kWh)	880.9	817.5	820.6
Electric Production CHP (kWh)	191.6	188.9	189.2
Thermal Efficiency of CHP	68.50%	66.22%	66.47%
Electric Efficiency of CHP	14.90%	15.30%	15.33%
Heat Production Boiler	849.0	875.0	771.6
Thermal efficiency of Boiler	76.59%	76.43%	76.43%
Heat losses (transmission + Fumes) (kWh)	890.9	881.8	746.1
Heat supplied for DHW(kWh)	20.7	21.5	19.9
Heat supplied for Heating (kWh)	1,291.2	1,287.3	1,288.8
Total energy discharged from TES (kWh)	13.6	13.5	0.4
Global Energy Efficiency	62.79%	62.94%	66.75%
Global Exergy Efficiency	13.33%	13.29%	13.81%
Hours of CHP in operation	168	168	168
ON/OFF cycles of Boiler	486	610	594
CO_2 emissions (kg)	435.8	433.1	408.4

Table 13. Different cases according to level ofthermal losses. (a) Cases of 15% and 10% of transmission losses. (b) Cases of 5% and 0 % of transmission losses.

	15% LOSSES		10% LOSSES	
	NON OPTIMIZED	OPTIMIZED	NON OPTIMIZED	OPTIMIZED
Micro-CHP fuel consumption (kWh_{LHV})	1,234.5	1,234.5	1,229.4	1,234.5
Boiler fuel consumption (kWh_{LHV})	1,089.0	927.2	951.6	857.5
Total of fuel (kWh_{LHV})	2,323.5	2,161.7	2,181.0	2,092.0
Heat Production CHP (kWh)	817.2	828.0	813.0	821.8
Electric Production CHP (kWh)	188.9	189.9	187.9	189.3
Thermal Efficiency of CHP	66.19%	67.07%	66.13%	66.57%
Electric Efficiency of CHP	15.30%	15.38%	15.28%	15.33%
Heat Production Boiler	832.2	708.6	727.2	655.3
Thermal efficiency of Boiler	76.42%	76.42%	76.42%	76.42%
Heat losses (transmission + Fumes) (kWh)	826.3	664.3	684.4	594.5
Heat supplied for DHW(kWh)	20.8	18.4	21.0	19.5
Heat supplied for Heating (kWh)	1,287.5	1,289.0	1,287.8	1,288.6
Total energy discharged from TES (kWh)	10	0.7	6.7	3.4
Global Energy Efficiency	64.44%	69.26%	68.62%	71.58%
Global Exergy Efficiency	13.59%	13.95%	14.42%	14.66%
Hours of CHP in operation	168	168	168	168
ON/OFF cycles of Boiler	587	538	512	490
CO_2 emissions (kg)	422.9	393.4	396.9	380.7

(a)

	5% LOSSES		0% LOSSES	
	NON OPTIMIZED	OPTIMIZED	NON OPTIMIZED	OPTIMIZED
Micro-CHP fuel consumption (kWh_{LHV})	1,219.2	1,229.4	1,183.1	1,188.2
Boiler fuel consumption (kWh_{LHV})	821.0	757.0	700.0	695.4
Total of fuel (kWh_{LHV})	2,040.2	1,986.4	1,883.1	1,883.6
Heat Production CHP (kWh)	802.5	818.4	776.2	773.2
Electric Production CHP (kWh)	185.8	188.4	179.2	179.5
Thermal Efficiency of CHP	65.82%	66.57%	65.60%	65.07%
Electric Efficiency of CHP	15.24%	15.32%	15.14%	15.11%
Heat Production Boiler	627.40	578.5	534.8	532.7
Thermal efficiency of Boiler	76.42%	76.42%	76.41%	76.60%
Heat losses (transmission + Fumes) (kWh)	545.6	490.0	394.3	394.6
Heat supplied for DHW(kWh)	20.9	19.7	21.8	23.4
Heat supplied for Heating (kWh)	1,288.0	1,288.2	1,287.8	1,286.1
Total energy discharged from TES (kWh)	12.9	11.3	54.6	219.4
Global Energy Efficiency	73.26%	75.33%	79.06%	79.05%
Global Exergy Efficiency	15.38%	15.41%	16.38%	16.85%
Hours of CHP in operation	168	168	168	167
ON/OFF cycles of Boiler	449	426	387	274
CO2 emissions (kg)	371.3	361.5	342.7	342.8

(b)

The CO_2 emissions that appear in the previous tables have been calculated with the factor 0.182 kg/kWh_{LHV} for Natural Gas, facilitated by [54].

To make a comparison between the non-optimized scenarios with different levels of thermal losses, the operational cost and exergy efficiency are contrasted. In terms of operational cost, comparing the non-optimized cases of 17% and 0% of thermal losses, a reduction of 24.39% is obtained. In relation to the exergy efficiency, contrasting the same cases, an increase of 23.25% is obtained by simply changing the level of thermal losses.

On the other hand, concerning the results of the optimized scenarios, it can be seen that the values for the new optimization variables in the real case give a reduction in the operational cost of 7.01% and an increment in the exergy efficiency of 3.91%.

As for storage use, it is worth noting how the optimized cases tend to reduce the use of storage until the level of transmission losses is close to 0%. Also worth noting is

the 0% transmission losses case, where there is a slight decrease in the energy efficiency, while there is an increase in the exergy efficiency; this is due to the optimization objective of increasing the exergy efficiency that aims to provide the heating and DHW at higher temperatures in order to increase the exergy provided. Thus, the latter objective is in direct opposition to the cost optimization objective, which will try to increase the energy efficiency by using a lower heating and DHW supply temperature so as to be able to use the available heat in the fumes as much as possible.

4 Conclusions

The work presented in this article analyses the behaviour of a hybrid installation composed of a Stirling based micro-CHP unit, a condensing boiler and an inertial tank. Experimental tests were carried out in the installation area present in the LCCE laboratory in Vitoria-Gasteiz, Spain. TRNSYS, a transient simulation software, was used to simulate a calibrated model of that experimental plant. Finally, the installation was optimized by means of a multi-objective optimization technique, using the NSGA-II algorithm. The main conclusions of the study are:

- In order to be able to use a computer model of an installation in the optimization process, it must be calibrated against the behaviour of the real operation. It has been proven that the use of a deterministic calibration approach is able to obtain a reduced CV(RMSE) error and provide a calibrated simulation model that behaves dynamically in a similar way to the real installation. The calibrated model also provides total fuel consumption and total heat and electricity production values similar to the real installation.

- A multi-objective optimization has been applied to the calibrated model of the installation with the aim of simultaneously maximizing the exergy efficiency and minimizing the operational cost of the plant for a one week operation. The variables modified to obtain the optimized configuration are five setting temperatures that define the operating mode of the plant. Applying the NSGA-II algorithm, a Pareto-frontier of non-dominated solutions is achieved. Through the decision-making method of minimum distance to the ideal point, it is proven that the selection of the control variables can provide a solution with a cost reduction of 7.01% and an increase of 3.91% in the exergy efficiency. Even if these improvements are similar to those obtained for optimizations of similar hybrid systems such as [29], they are in the order of magnitude of the typical operational uncertainty of this type of systems.
- In the analysed hybrid system, the cost reduction optimization was directly linked to the reduction of fuel consumption and, thus, to the reduction of CO_2 emissions. For other types of hybrid system, the environmental objectives might not be directly linked to the reduction of fuel consumption alone, in which case the CO_2 emissions should be considered explicitly in the multi-objective optimization process.
- Considering the above issues, the presented methodology for hybrid systems model calibration, validation and control strategy optimization, could be extensible to other types of in-use hybrid systems.
- Without changing the parameters of the control logic, the cost of operation can be reduced by 24.39%, if the insulation were ideal and the thermal losses were zero. For this ideal case, the exergy efficiency would improve by 23.25%. If the thermal insulation is only changed to reach 5% of transmission losses, the reduction in consumption is 14.26% and the increase in exergy efficiency is 15.64%. Thus, the

correct insulation of the installation is more important than the effect of the control variables on this type of installation. Note that this research has assumed that the transmission losses are not used, but in some real cases, part of those transmission losses might occur within the building and would then be equivalent to space heating supply. Thus, when optimizing real hybrid installations, the transmission losses that are used as heating should not be considered as transmission losses.

- Regarding the thermal storage use, analysing the results of the different optimizations, it is seen that when the losses are considerable, it makes no sense to use thermal storage. However, if the losses are negligible, the optimized scenario tends to drastically increase the use of the thermal storage system.
- Finally, from the analysis of the levels of thermal losses, it can be concluded that the cost or energy optimizations that optimize the adiabatic model of this hybrid system is insensitive to the selected control variables. This is extensible to periods where the Stirling engine would be working continuously.

Further work in this field should include a whole year study, as this case has used just the week of the year with the highest demand to calibrate, validate and optimize the hybrid installation. The calibrated model should be checked against a medium demand week in spring or autumn and against an only DHW demand week in summer. This model could then be used to perform a whole year optimization analysis. It must be noted that, with the need to use a 10 second time-step due to the fast answer of the hybrid installations, the yearly calculations would be computationally extremely demanding.

Acknowledgement

This work was supported by the Spanish Economy and Competitiveness Ministry and the European Regional Development Fund through the IMMOEN project

'Implementation of automated calibration and multi-objective optimization techniques applied to Building Energy Model simulations by means of monitored buildings', project reference: ENE2015-65999-C2-2-R and ENE2015-65999-C2-1-R (MINECO/FEDER); by the Spanish Ministry of Science, Innovation and Universities and the European Regional Development Fund through the MONITHERM project 'Investigation of monitoring techniques of occupied buildings for their thermal characterization and methodology to identify their key performance indicators', project reference: RTI2018-096296-B-C22 (MCIU/AEI/FEDER, UE).

Special acknowledgements to the Laboratory for Quality Control in Buildings (LCCE) of the Basque Government for providing the opportunity to use their installation area for the tests carried out in this research.

References

[1] Eurostat. Recast, E.P.B.D. Directive 2010/31/EU of the European Parliament and of the Council of 19 May 2010 on the Energy Performance of Buildings; Official Journal of the European Union (OJ): Brussels, Belgium, 2010. Statistics database, energy statistics and supply, transformation, consumption (2010).
[2] Ministry of Industry Tourism and Commerce Government of Spain.

Eurostat European Commission, IDAE, SECH-SPAHOUSEC project, Institute for Energy Diversification and Saving. (2011).
[3] Q. Zhai, H. Cao, X. Zhao, C. Yuan. Assessing application potential of clean energy supply for greenhouse gas emission mitigation: a case study on General Motors global manufacturing. Journal of Cleaner Production. 75 (2014) 11-9.
[4] H.I. Onovwiona, V.I. Ugursal. Residential cogeneration systems: review of the current technology. Renewable and Sustainable Energy Reviews. 10 (2006) 389-431.
[5] V. Kuhn, J. Klemeš, I. Bulatov. MicroCHP: Overview of selected technologies, products and field test results. Applied Thermal Engineering. 28 (2008) 2039-48.
[6] V. Dorer, A. Weber. Energy and CO2 emissions performance assessment of residential micro-cogeneration systems with dynamic whole-building simulation programs. Energy Conversion and Management. 50 (2009) 648-57.
[7] T.Z. Kaczmarczyk, G. Żywica, E. Ihnatowicz. Experimental study of a low-temperature micro-scale organic Rankine cycle system with the multi-stage radial-flow turbine for domestic applications. Energy Conversion and Management. 199 (2019) 111941.
[8] D. Zhang, S. Evangelisti, P. Lettieri, L.G. Papageorgiou. Optimal design of CHP-based microgrids: Multiobjective optimisation and life cycle assessment. Energy. 85 (2015) 181-93.
[9] H. Hachem, R. Gheith, F. Aloui, S. Ben Nasrallah. Technological challenges and optimization efforts of the Stirling machine: A review. Energy Conversion and Management. 171 (2018) 1365-87.
[10] A.C. Ferreira, M.L. Nunes, J.C.F. Teixeira, L.A.S.B. Martins, S.F.C.F. Teixeira, S.A. Nebra. Design of a solar dish Stirling cogeneration system: Application of a multi-objective optimization approach. Applied Thermal Engineering. 123 (2017) 646-57.
[11] D.G. Thombarse. Stirling Engine: Micro-CHP System for Residential Application. Encyclopedia of Materials: Science and Technology (Second Edition). (2008).
[12] R. Evins. A review of computational optimisation methods applied to sustainable building design. Renewable and Sustainable Energy Reviews. 22 (2013) 230-45.
[13] A. Frangioni, C. Gentile, F. Lacalandra. Tighter Approximated MILP Formulations for Unit Commitment Problems. IEEE Transactions on Power Systems. 24 (2009) 105-13.
[14] V. Senthil Kumar, M.R. Mohan. Solution to security constrained unit commitment problem using genetic algorithm. International Journal of Electrical Power & Energy Systems. 32 (2010) 117-25.
[15] C. Christober, R. Asir. An evolutionary programming based simulated annealing method for unit commitment problem with cooling-banking constraints. Proceedings of the IEEE INDICON 2004 First India Annual Conference, 20042004. pp. 435-40.

[16] A. Bhardwaj, K. Vikram Kumar, S. Vijay Kumar, B. Singh, P. Khurana. Unit commitment in electrical power system-a literature review. 2012 IEEE International Power Engineering and Optimization Conference Melaka, Malaysia2012. pp. 275-80.
[17] Z. Ouyang, S.M. Shahidehpour. An intelligent dynamic programming for unit commitment application. IEEE Transactions on Power Systems. 6 (1991) 1203-9.
[18] L. Tao, M. Shahidehpour. Price-based unit commitment: a case of Lagrangian relaxation versus mixed integer programming. IEEE Transactions on Power Systems. 20 (2005) 2015-25.
[19] H. Sayyaadi, M. Nejatolahi. Multi-objective optimization of a cooling tower assisted vapor compression refrigeration system. International Journal of Refrigeration. 34 (2011) 243-56.
[20] V. Jain, G. Sachdeva, S.S. Kachhwaha, B. Patel. Thermo-economic and environmental analyses based multi-objective optimization of vapor compression–absorption cascaded refrigeration system using NSGA-II technique. Energy Conversion and Management. 113 (2016) 230-42.
[21] R. Wang, G. Li, M. Ming, G. Wu, L. Wang. An efficient multi-objective model and algorithm for sizing a stand-alone hybrid renewable energy system. Energy. 141 (2017) 2288-99.
[22] K. Deb, A. Pratap, S. Agarwal, T. Meyarivan. A fast and elitist multiobjective genetic algorithm: NSGA-II. IEEE Transactions on Evolutionary Computation. 6 (2002) 182-97.
[23] N. Delgarm, B. Sajadi, S. Delgarm, F. Kowsary. A novel approach for the simulation-based optimization of the buildings energy consumption using NSGA-II: Case study in Iran. Energy and Buildings. 127 (2016) 552-60.
[24] X. Chen, H. Zhou, W. Li, Z. Yu, G. Gong, Y. Yan, et al. Multi-criteria assessment and optimization study on 5 kW PEMFC based residential CCHP system. Energy conversion and management. 160 (2018) 384-95.
[25] F. Bre, V.D. Fachinotti. A computational multi-objective optimization method to improve energy efficiency and thermal comfort in dwellings. Energy and Buildings. 154 (2017) 283-94.
[26] G. Ding, W. Chen, T. Zheng, Y. Li, Y. Ji. Volume ratio optimization of Stirling engine by using an enhanced model. Applied Thermal Engineering. 140 (2018) 615-21.
[27] G. Xiao, Y. Huang, S. Wang, H. Peng, M. Ni, Z. Gan, et al. An approach to combine the second-order and third-order analysis methods for optimization of a Stirling engine. Energy Conversion and Management. 165 (2018) 447-58.
[28] E.S. Barbieri, F. Melino, M. Morini. Influence of the thermal energy storage on the profitability of micro-CHP systems for residential building applications. Applied Energy. 97 (2012) 714-22.
[29] K. Alanne, N. Söderholm, K. Sirén, I. Beausoleil-Morrison. Techno-economic assessment and optimization of Stirling engine micro-cogeneration systems in residential buildings. Energy Conversion and Management. 51 (2010) 2635-46.
[30] S. Klein. TRNSYS 17—A Transient System Simulation Program User Manual University of Wisconsin-Madison, Solar Energy Laboratory, Madison, WI, USA2012.
[31] Ministry of development Government of Spain. CTE, 2013a, Technical Building Code, Basic Document HE Energy Saving. Section HE1 Limitation of energy demand (2013).
[32] L.M. López-Ochoa, J. Las-Heras-Casas, L.M. López-González, P. Olasolo-Alonso. Towards nearly zero-energy buildings in Mediterranean countries: Energy Performance of Buildings Directive evolution and the energy rehabilitation challenge in the Spanish residential sector. Energy. 176 (2019) 335-52.
[33] Ministry of development Government of Spain. CTE. Technical Code for Building. (2013).
[34] Ministry of development Government of Spain. CTE, 2013b, Technical Building Code, Basic Document HE Energy Saving. Section HE4: Minimum solar contribution of domestic hot water (2013).
[35] U. Jordan, K. Vajen. DHWcalc: Program to generate domestic hot water profiles with statistical meand for user defined conditions. ISES Solar World Congress. (2005) 1-6.

[36] D. Haeseldonckx, L. Peeters, L. Helsen, W. D'haeseleer. The impact of thermal storage on the operational behaviour of residential CHP facilities and the overall CO2 emissions. Renewable and Sustainable Energy Reviews. 11 (2007) 1227-43.
[37] J.N. De Wit, M. Mini and micro cogeneration. Proceedings of the 17th international energy and environment fair and conference (ICCI 2011), Istanbul, Turkey, 2011.
[38] A. Campos Celador, M. Odriozola, J.M. Sala. Implications of the modelling of stratified hot water storage tanks in the simulation of CHP plants. Energy Conversion and Management. 52 (2011) 3018-26.
[39] G. Rey, C. Ulloa, J.L. Míguez, E. Arce. Development of an ICE-based micro-CHP system based on a stirling engine; methodology for a comparative study of its performance and sensitivity analysis in recreational sailing boats in different European climates. Energies. 9 (2016).
[40] V. Malaguti, C. Lodi, M. Sassatelli, S. Pedrazzi, G. Allesina, P. Tartarini. Dynamic behavior investigation of a micro biomass CHP system for residential use. International Journal of Heat and Technology. 35 (2017) S172-S8.
[41] I. Gonzalez-Pino. Modelling, experimental characterization and simulation of stirling engine-based micro-cogeneration plants for residential buildings. Universidad del País Vasco-Euskal Herriko Unibertsitatea2019.
[42] R. Hendron, J. Burch, G. Barker. Tool for Generating Realistic Residential Hot Water Event Schedules. Simbuild 2010: Proceedings of the 4th National Conference of IBPS-USA, 2010.
[43] A. González-Gil, J.L. López González, M. Fernández, P. Eguía, A. Erkoreka, E. Granada. Thermal energy demand and potential energy savings in a Spanish surgical suite through calibrated simulations. Energy & Buildings. 174 (2018) 513-26.
[44] A. Cacabelos, P. Eguía, L. Febrero, E. Granada. Development of a new multi-stage building energy model calibrationmethodology and validation in a public library. Energy and Buildings. 146 (2017) 182-99.
[45] GENOPT Generic Optimization Program. Lawrence Berkeley National Laboratory, University of California, http://simulationresearch.lbl.gov/GO/. p. Last accessed December 2018.
[46] M. Fernández, P. Eguía, E. Granada, L. Febrero. Sensitivity analysis of a vertical geothermal heat exchanger dynamic simulation: Calibration and error determination. Geothermics. 70 (2017) 249-59.
[47] M.D. Morris. Factorial Sampling Plans for Preliminary Computational Experiments. Technometrics. 33 (1991) 161-74.
[48] J.H. Holland. Genetic Algorithm, Scientific American. 253 (1992) 66.
[49] JEPlus. An EnergyPlus simulation manager for parametrics. http://www.jeplus.org/wiki/doku.php?id=start. p. Last accessed September 2018.
[50] R.A. Lara, E. Naboni, G. Pernigotto, F. Cappelletti, Y. Zhang, F. Barzon, et al. Optimization Tools for Building Energy Model Calibration. Energy Procedia2017. pp. 1060-9.
[51] X. Chen, H. Yang, K. Sun. A holistic passive design approach to optimize indoor environmental quality of a typical residential building in Hong Kong. Energy. 113 (2016) 267-81.
[52] S. Carlucci, G. Cattarin, F. Causone, L. Pagliano. Multi-objective optimization of a nearly zero-energy building based on thermal and visual discomfort minimization using a non-dominated sorting genetic algorithm (NSGA-II). Energy and Buildings. 104 (2015) 378-94.
[53] H. Sayyaadi, G. Ghorbani. Conceptual design and optimization of a small-scale dual power-desalination system based on the Stirling prime-mover. Applied Energy. 223 (2018) 457-71.
[54] Ministry of agriculture and fishing, food and environment. Spanish Government. Factores de emisión. Registro de huella de carbono, compensación y proyectos de absorción de dioxido de Carbono. (2018).